UNIVERSITY OF SOUTHAMPTON

FACULTY OF MEDICINE

School of Clinical and Experimental Sciences

Measuring the Pressure of the Intervertebral Disc

by

Amr Fahmy

Thesis for the degree of Doctorate in Medicine

March 2013

University of Southampton

ABSTRACT

FACULTY OF MEDICINE

Doctorate of Medicine

by Amr Fahmy

Spinal musculoskeletal conditions are an economical burden; in the United States alone, the annual cost of these conditions is estimated to be $254 billion. These conditions are also a social burden; in the United States, for example, musculoskeletal problem is the number one reason for a visit to a physician. Most of these conditions are caused by degenerative changes in the vertebral column. Such degenerations are, often, the result of long-term *changes in the intervertebral disc pressure*. To date, the standard methodology to measure this pressure suffers from being invasive, which prevents it from being widely applicable. Thus, developing a validated, non-invasive method for measuring the intervertebral disc pressure can be a valuable diagnostic tool.

An ideal, non-invasive, solution to measure the pressure of the intervertebral disc would be to use MRI scanners; they are safe and widely available. To date, however, there have been no studies to validate, or invalidate, this proposal. Thus, the main goal of the dissertation is to provide the corner stone for studying this proposal. To this end, the proposed approach consists of three steps: (1) measuring the pressure within the intervertebral disc, (2) obtaining an MR image for the same disc, and (3) comparing the two and finding whether a link exists between them. This dissertation contributes towards the first step by developing, and validating, a layout suitable for in-vitro application to spinal motion segments.

Table of Content

List of Figures

Acknowledgements

First of all, I would like to express my sincere gratitude to my supervisor, Dr. Hamid Rassoulian, who has helped to shape this research from the very first day, and always has been supportive and patient throughout the whole period of my study until the very last day before submission.

I would like to thank my family, especially my wife, Hanan, who had to go through the difficult times helping me to fulfil my ambition, and for being so kind, patient, loving, caring, cheerful, and most importantly, for being the greatest mother for my children.

I would also like to thank my close friend, Dr. A. Aziz, who has always understood me and cheered me up whenever I felt uneasy.

Finally, I would like to thank all my colleagues for their endless support.

To my wife, Hanan, for being always by my side when I needed her most.

Chapter 1

Introduction

Spinal musculoskeletal conditions are a social and financial burden for both the individuals as well as society. In the United States alone, the annual cost of such conditions is estimated to be $254 billion [Terry Canale and Beaty, 2007]. Although these conditions are generally not fatal, they are often chronic. In the United States, for example, musculoskeletal problems are the number one reason for a visit to a physician, and lower back pain is by far the most frequent musculoskeletal complaint. Axial spine pain—whether cervical, thoracic, or lumbar—is often attributed to disc degeneration. As is the case with other degenerative processes, disc degeneration does not always cause pain at its early stages. However, it can lead to internal disc derangement otherwise known as disc herniation. Each pathological process has unique clinical findings and treatments. Against this background, the focus in this dissertation will be on the intervertebral disc.

The human intervertebral disc is known to be a relatively complex fibro-collagenous structure, permitting load bearing, limiting excessive motion between adjacent vertebrae, and maintaining anatomic relationships of surrounding bony and ligamentous structures [Skaggs et al., 1994]. Mechanical failures of the intervertebral discs are often associated with various spinal pathologies. It has been shown that such failures are strongly linked to the pressure changes of a certain intervertebral disc component known as the nucleus pulposus [Nachemson, 1966]. To date, the standard methodology for measuring the intervertebral disc pressure suffers from major

limitations that prevent it from being widely applicable, and this dissertation contributes towards overcoming these limitations.

The remainder of this chapter is structured as follows. Section 1.1 introduces the mechanical model of the intervertebral disc and spinal motion segment. Section 1.2 outlines the research aims and objectives. Finally, Section 1.3 gives the overall structure of this dissertation.

1.1 Clinical Relevance, the Problem and the Purpose

The accepted anatomical and mechanical model of the intervertebral disc consists of a liquid *nucleus pulposus* (NP) surrounded and constrained by the concentric lamellae of an elastic *annulus fibrosus* (AF) and two, superior and inferior, *cartilaginous end plates* (CP) [Mc Nally and Adams, 1992]. This is illustrated in Figure 1.1 [Terry Canale and Beaty, 2007]. The nucleus pulposus is gelatinous in humans, with high viscosity and elasticity. It comprises a three-dimensional structure of protoglycan, as well as intermolecular free water [Sato et al., 1999].

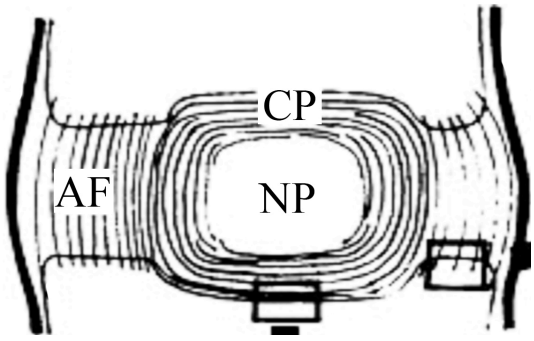

Figure 1.1 Schematic representation of orientation of fibers in disc and endplate. *AF:* Annulus fibrosus; *NP:* nucleus pulposus; *CP:* cartilaginous plate. (Adopted from Terry Canale and Beaty, 2007)

The nucleus pulposus exhibits hydrostatic properties due to its high water content [Hendry, 1958]. In more detail, the nucleus pulposus resists the compressive forces by the increase in its internal pressure, as well as the high tensile stresses on the annulus [Hutton, 1999]. This increase

in pressure within the disc causes an increase in the disc cell metabolism and nutrition [Hutton, 1999].

It has been accepted—based on clinical backgrounds—that an increase in the pressure within the nucleus pulposus (e.g., by injecting contrast media while performing provocative discography) induces pain whenever the disc is abnormal [Kim et al., 2009]. It has also been suggested that a wide range of spinal pathologies—including spinal instability and disc degenerative diseases—are all related to earlier changes in the intervertebral disc pressure [Sato et al., 1999]. Aging and degenerative changes of the intervertebral disc include annular changes, nuclear changes or, in most cases, both together. In more detail, annular changes include the loss of annular integrity, fraying, splitting and loss of collagen fibers within the annulus, resulting in annular peripheral tears and alteration in the entire disc biomechanics. Nuclear changes, on the other hand, are often associated with fibrosis and complex biochemical changes as well as dehydration of the nucleus, which is directly related to the intervertebral disc pressure changes [Mirza and White, 1995].

Compere [1961] concluded that high stresses, which are most obvious in the lower lumbar vertebrae, result in degenerative changes in the intervertebral discs, such as fibrillations and cracking in both the endplates and the annulus. These changes cause the nucleus pulposus material to be extruded out of the disc space. Specifically, whenever the spine is flexed (e.g., during lifting, twisting or bending) the degenerated nucleus is compressed against the thin posterior annulus fibres and consequently breaks through the thin annulus fibres and extrudes into the spinal canal causing nerve root irritation (see Figure 1.2). This extrusion results in the following changes in the intervertebral discs: (1) disc space narrowing, (2) drop in disc pressure which, in turn, results in a softer disc, and (3) further dehydration of the residual part of the nuclear material. These changes negatively affect the ability of the intervertebral disc to function as a shock absorber, as an insulator between two vertebral bodies and as an axis of motion for the vertebral articulation. Thus the two vertebrae, along with the degenerated disc in-between, soon start to show signs of wear-and-tear, otherwise known as sclerosis and osteophyte formation, which are clinical observations that are widely recognized.

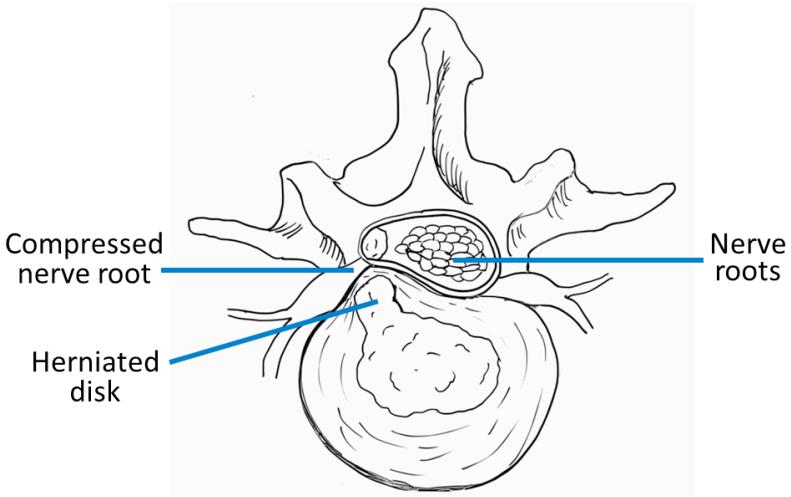

Figure 1.2 Diagram of herniated disc material causing nerve root irritation.

Compere [1961] was able to repeat the disc degeneration process detailed above in both dogs and monkeys by allowing some of the nucleus material to escape through a relatively small opening in the annulus. Another study of the same pathological process was carried out by Boutin and Hogshead [1992]. In particular, their study included 508 patients who had discectomy for disc degenerative disorders. They found that, in 85% of the cases, the extruded material was purely nucleus, while in the remaining 15% the material was found to be a mixture of both nucleus and annulus [Boutin and Hogshead, 1992].

The disc pressure is a direct reflection of the loads to which the motion segment of the spine is subjected [Nachemson, 1981]. Experiments and studies done by Nachemson during the 1960s and 1970s are considered to be the corner stone of almost all disc pressure studies [Sato et al., 1999]. These studies demonstrated variations in the disc pressure when performing various tasks and adopting different working positions, e.g., standing, sitting and lifting [Nachemson, 1981; Adams and Hutton, 1983; Wilke et al., 1999]. The same studies also demonstrated that compressive loading is the major determinant of the disc pressure changes.

The link between the change in intervertebral disc pressure and the degree of disc degeneration has been accepted [Panjabi et al., 1988]. Based on this, providing a non-invasive technique for measuring the intervertebral disc pressure would be a clinically valuable tool, especially since most existing radiological technologies accepted for spinal diagnosis may fail to identify abnormalities in spinal patients. To date, however, all studies conducted since the 1960s relied on invasive procedures to measure and monitor the changes in intervertebral disc pressure. This has limited the clinical use and application of pressure recordings. Developing a validated, non-invasive alternative would make the clinical use and application of the intervertebral disc pressure recordings more feasible and consequently provide a better understanding of the nature, functions, biomechanical properties and pathology of the intervertebral disc.

In more detail, in clinical practice, it is not uncommon for spinal patients to complain from genuine symptoms, with lack of positive findings upon investigations. These investigations may include plain radiographs, CT scans or MRI scans. In such situation, the only available next step would be to perform an invasive procedure to estimate the intervertebral disc pressure and assess its integrity. This invasive procedure is known as “the provocative discography”. Even with this procedure, results may be falsely negative. Such a situation becomes even more complicated in medicolegal litigations. Clearly, it would be ideal to provide pressure modelling that can be used for any future work that aims at estimating the pressure reading from images generated using the MRI scanners.

1.2 Research Aims and Objectives

Being non-invasive, safe and widely available, MRI scanners provide the best modality for studying the intervertebral disc pathologies. What would be desirable, then, is to be able to use these scanners to measure the pressure of the intervertebral disc. This would provide the ideal solution to overcome the limitations of invasive pressure measurement methods. To date, however, there have been no studies to validate, or invalidate, this proposal. Against this

background, the main goal of this dissertation is to provide the corner stone for studying this proposal. The proposed approach consists of three main steps: (1) measuring the pressure within the intervertebral disc in a spinal motion segment, (2) obtaining an MR image for the same specimen, and (3) comparing the two and finding whether a link exists between them. This dissertation contributes towards the first step of the aforementioned approach. The following milestones have been set:

- Develop and validate a pressure sensor layout suitable for in-vitro application to animal specimen.
- Develop and validate an experimental protocol for measuring the pressure in the specimens using the sensor.
- Validate the proposed pressure sensor layout through different validation methodologies.
- Conduct experiments on specimens (i.e., spinal motion segments), where pressure within the intervertebral disc is first measured in neutral position (i.e., in a position where no deformation is applied). After that, quantitative, reproducible deformations are applied, and changes in disc pressure are recorded, so as to verify whether the aforementioned deformations are reflected in the pressure readings.

The above contributions lay the basic foundations for developing a validated, non-invasive, method for measuring the pressure of the intervertebral disc.

1.3 General Layout of the Dissertation

In this dissertation, related literature is reviewed, a new kit for measuring the pressure of intervertebral discs is assembled, and experiments are conducted and analysed. This is achieved through the course of the remaining chapters, which are structured as follows:

- Chapter 2 discusses the existing literature, focusing on the studies that are related to the development and embryological origin of the vertebral column. It also studies the anatomy of the vertebral column as a whole, including the intervertebral discs, its

biomechanical features and blood and nerve supply. Finally it outlines the previously reported work related to intervertebral disc pressure measurement.

- Chapter 3 discusses the ethics of using the animal tissues for scientific research purposes. It then acknowledges the differences between human and animal spinal specimens. These include (1) differences in the development of the spinal segments, (2) differences due to anatomical variations, (3) differences due to biomechanical variations, and (4) differences while loading the spinal segments and intervertebral discs. Finally, the chapter discuses different aspects of the process of storing animal specimens for research purposes.

- Chapter 4 discusses the basic principles of pressure and its measurements. After that, it describes pressure sensor layout and validates it using two different methods: with and without a calibrator. Finally, experiments are conducted to verify whether a deformation in the spinal motion segment is reflected by the pressure sensor readings.

- Finally, Chapter 5 concludes this dissertation, focusing on the advantages of the proposed tool and outlining future work that can be carried out to extend and enhance this tool.

Chapter 2

Background and Survey of Literature

This chapter surveys the relevant literature. Specifically, Section 2.1 looks at the development of the vertebral column and intervertebral discs. After that, Section 2.2 describes the anatomical details of the vertebral column. Section 2.3 provides a detailed description of the components of the intervertebral disc. Finally, Section 2.4 outlines the previous work related to intervertebral disc pressure measurement.

2.1 Development of the Vertebral Column and Intervertebral Discs

Generally, the skeleton is considered to be formed by two main parts: (1) the axial and (2) the appendicular. In more detail, the axial skeleton includes cranium, vertebral column, and their associated thoracic cage formed of sternum, costal cartilages and ribs. Appendicular skeleton include the limbs. In vertebrata, a stiff and flexible axis is essential. Therefore, a chain of bones connected by the discs of deformable substances develops around the vital structures and protects them. The vertebral elements are complex and vary in structure. The most basic part is the *centrum,* which forms most of the vertebral bodies, anterior to the spinal cord. Typically, a *vertebral foramen*, enclosing the spinal cord, fuses anteriorly with the centrum and usually bears a median spinous process and paired lateral transverse processes (see Figure 2.1) [Moore et al., 2008].

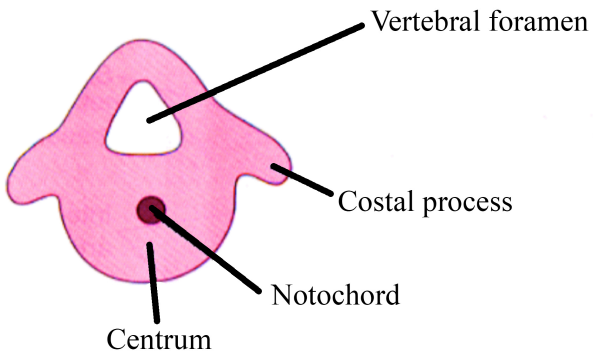

Figure 2.1 Basic elements of the vertebra formed of the centrum and the vertebral foramen. (Reproduced with permission from Moore et al, The Developing Human Clinically oriented embryology, 2008)

The intervertebral disc (IVD) is considered to be the principal component of the vertebral articulation. IVDs were recognized as an anatomical entity by Andreas Vesalius (1514-64). The major role of IVDs is mechanical, as they constantly transmit loads arising from body weight and muscle activity through the vertebral column [Compere, 1961]. They also provide flexibility, allowing bending, torsion, and flexion. Generally, along the entire length of the vertebral column, a total of twenty-five IVDs are interposed between the adjacent vertebrae, which unite them from the first cervical vertebra- known as the *Axis* down to the *Sacrum*. In the lumbar region of the spine, each IVD is approximately 7 to 10 mm thick, 4 cm in diameter, and consists of three integrated tissues, namely the Nucleus Pulposus (NP), the Annulus Fibrosus (AF), and the Cartilage End Plates (CEP) as shown in (Figure 2.2) [Prithvi-Raj, 2008].

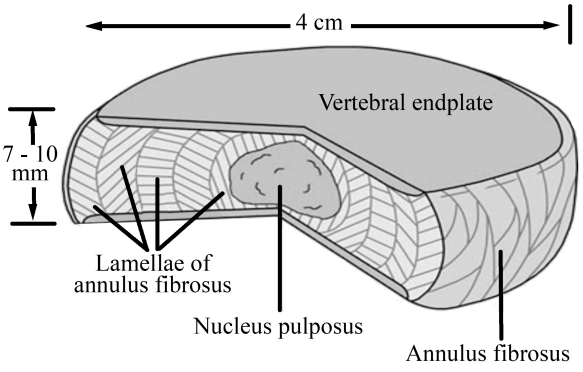

Figure 2.2 Illustration showing the gross structure and diameter of lumbar IVD. (Adoped from Prithvi-Raj, 2008)

Each disc is anchored to its adjacent vertebrae by the attachments of the Cartilage End Plate (*CEP*) and the Annulus Fibrosus (*AF*). An IVD, with its subjacent vertebral bodies and associated ligaments, constitutes what is known as "*the spinal motion segment*". Throughout this dissertation, the term "*spinal motion segment*" will be used to describe intervertebral disc, with its adjacent vertebral bodies and their associated ligaments, which is the basic functional concept for experimental investigations of the IVD (see Figure 2.3) [Prithvi-Raj, 2008].

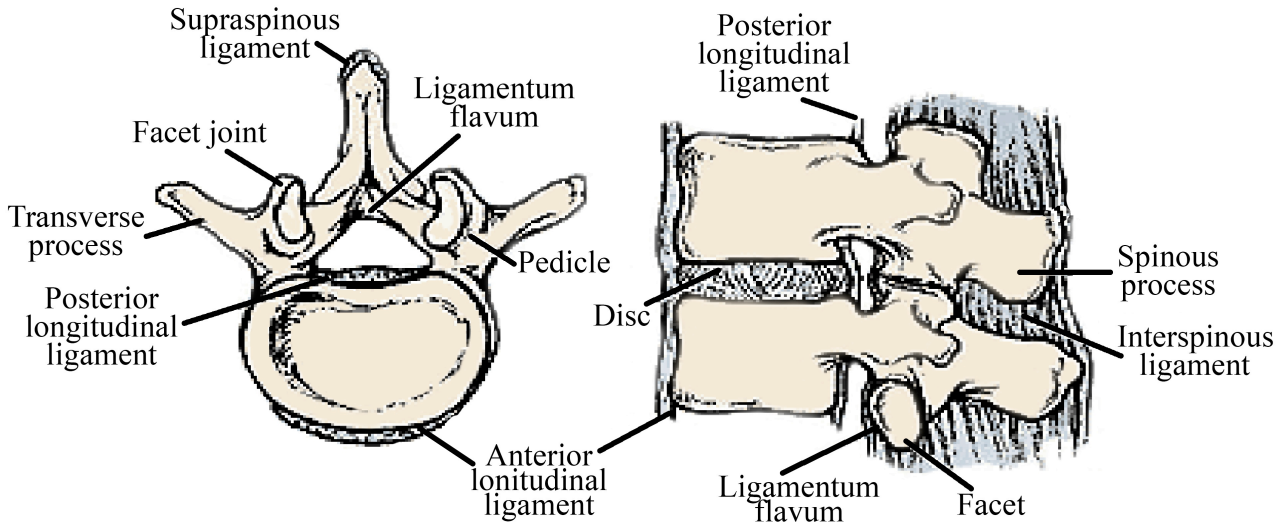

Figure 2.3 Anatomy of a spinal motion segment: two vertebrae, one intervertebral disc, and ligaments (Adoped from Prithvi-Raj, 2008)

Along the entire length of the vertebral column, the longitudinal ligaments (anterior and posterior) are attached to the vertebral bodies respectively. The Anterior Longitudinal Ligament (ALL) is firmly attached to the periosteum of the vertebral bodies. However, it is not attached to the IVDs. The Posterior Longitudinal Ligament (PLL) has its distinct denticulate appearance with extensions over the IVDs to which it is firmly attached. The PLL is narrowest over the vertebral bodies, and is separated from them by the emerging basivertebral vessels [Drake et al., 2010].

2.1.1 Development of the Vertebral Column

This section describes the embryological development of the vertebral column. In particular, Section 2.2.1.1 discusses the somites and their generation. Section 2.2.1.2 discusses the development of the vertebrae from the somites. Section 2.2.1.3 discusses the development of chondrification centres and ossification centres. Finally, Section 2.2.1.4 discusses the vertebral growth and the development of secondary ossification centres.

2.1.1.1 Somitogenesis

Somites are considered as the basic subunits to form the skeletal system. They are generated from the pre-somatic mesenchyme. The segmentation of the para-axial pre-somatic mesenchyme occurs as a sequential process along the cranio-caudal axis. In an embryo, a pair of somites is formed every 90 minutes.

Two important structures are formed during the third week of gestation: the notochord and the neural tube. In particular, the neural tube is formed by the fusion of the neural folds (see Figure 2.4) [Moore et al., 2008]. The embryonic mesoderm lateral to these two structures forms two longitudinal columns known as the *para-axial mesoderm*. Towards the end of the third week, the dorso-lateral columns of the para-axial mesoderm are segmented into mesodermal blocks through the process of *segmentation* and start to form the somites. After that, the para-axial mesoderm migrates laterally to the notochord. The bony vertebral column and its associated muscles are then formed from these para-axial mesenchyme cells. The somites provide the embryonic cell population for the bones and muscles.

Somites develop and differentiate into two parts:

- *Sclerotome*, which is responsible for the development of the vertebrae and ribs. It lies on the ventral-medial aspect of the developing embryo.
- *Dermo-myotome*, which is found on the dorsal-lateral aspect. Its myotome part forms the myoblasts, while its dermatome part forms dermis.

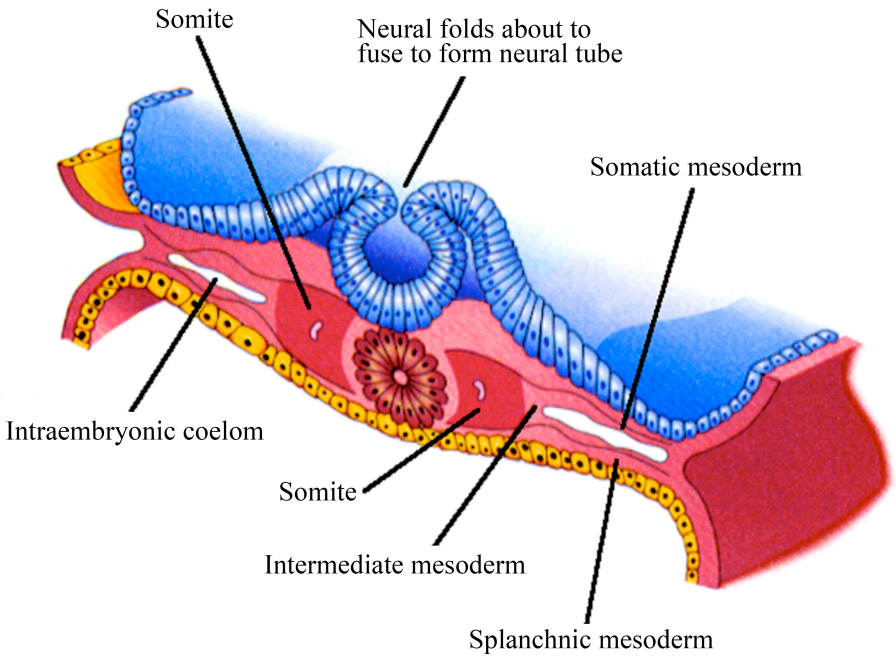

Figure 2.4 Transverse section in a 22 days embryo showing the appearance of early somites. The neural tube is about to fold to form the neural tube. (Reproduced with permission from Moore et al, The Developing Human Clinically oriented embryology, 2008)

2.1.1.2 Vertebrae and Intervertebral Discs

During the vertebral column development, intersegemental fissures—known as the von Ebner's fissures—appear within the sclerotome. These fissures divide the sclerotome into two halves: a loosely packed cranial half, and a densely packed caudal half (Figure 2.5 [Moore et al., 2008]).

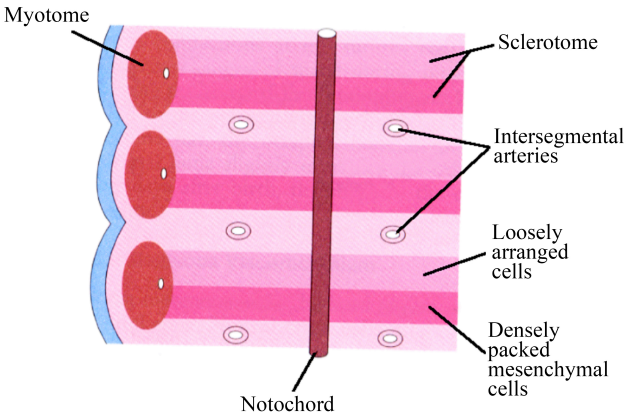

Figure 2.5 Diagrammatic section of embryo-showing condensation of the sclerotomal cells around the notochord. (Reproduced with permission from Moore et al, The Developing Human Clinically oriented embryology, 2008)

The bilateral sclerotome cell population migrates towards the notochord, surrounds it, and forms the *perinotochordal sheath*. Those cells then differentiate "chondrogenetically" to form the cartilaginous precursor of the vertebral centrum. The caudal, densely-packed cells fuse with the loosely arranged cells of the adjacent sclerotome. By so doing, they form the *mesenchymal centrums,* which are the primordium for the vertebral bodies. Each centrum then develops to from two adjacent sclerotomes. Those two fuse together giving rise to a single vertebral body. An illustration is provided in figures 2.5 and 2.6 [Moore et al., 2008].

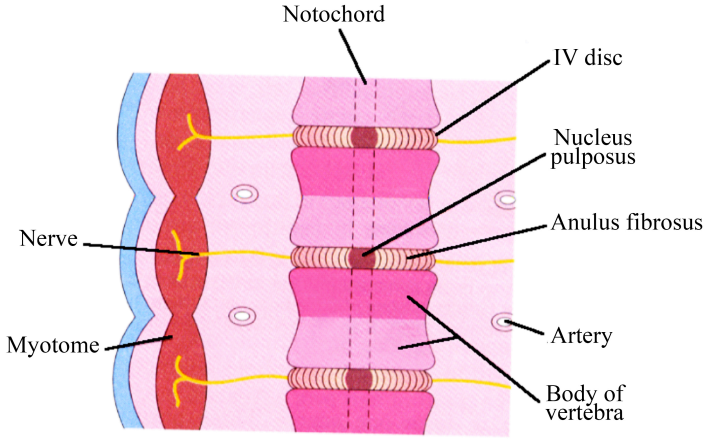

Figure 2.6 Diagrammatic frontal section illustrating the vertebral body formed from cranial and caudal halves of two adjacent sclerotomes. (Reproduced with permission from Moore et al, The Developing Human Clinically oriented embryology, 2008)

At the site of the vertebral bodies, the part of the notochord that is surrounded by a vertebral body starts to degenerate and eventually disappears. As for the remaining part of the notochord, it expands to form the gelatinous centre for the nucleus pulposus.

2.1.1.3 Chondrification Centres and Primary Ossification Centres

During the sixth week of embryonic life, chondrification centres appear in each mesenchymal vertebra (see Figure 2.7) [Moore et al., 2008]. Two centres fuse by the end of the embryonic period to form the cartilaginous centrum. Concomitantly, centres in the neural arches also fuse with the cartilaginous centrum. The transverse and spinous processes of the vertebra then

develop as extensions of these chondrification centres. Chondrification spreads until the cartilaginous vertebral column is formed.

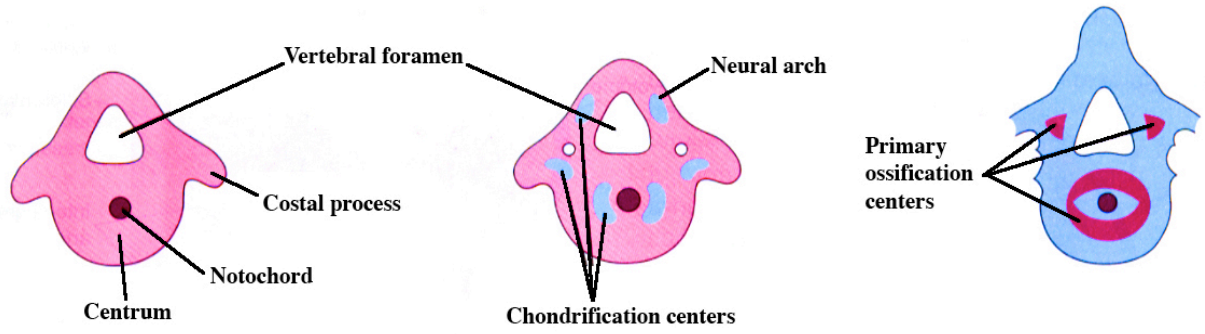

Figure 2.7 Chondrification centres appear in the mesenchymal vertebra. Primary Ossification centres develop at the end of the embryonic life. (Adopted from Standring et al., 2005)

The ossification of the vertebrae normally starts during the intrauterine period. It continues until the age of 25 years. Three primary ossification centres appear by the end of the embryonic development: one at the centrum and two on the sides of the neural foramen. At the time of birth, each vertebra will be formed of three bony parts connected by cartilage, one body and two halves of the neural arch (see Figure 2.7) [Moore et al., 2008].

2.1.1.4 Vertebral Growth and Secondary Ossification Centres

Each half of the bony vertebra fuses with its counterparts during the first three to five years of life. The fusion process starts at the lumbar region and progresses cranially. Vertebral arches articulate with the centrum at the cartilaginous neurocentral joints. These joints permit the vertebral arches to grow as the spinal cord enlarges. The vertebral arches then fuse with the centrum, and the neurocentral joints disappear during the third to sixth year of life. After puberty, five secondary ossification centres appear in each vertebra. They are situated at the following points:

(1) One centre is situated at the tip of the spinous process.
(2) One centre is situated at the tip of each transverse process.
(3) Two centres are situated at the annular epiphysis; one on the superior rim and the other on the inferior rim of the vertebral body (see Figure 2.8) [Moore et al., 2008].

The vertebral body is formed of the annular epiphyses and the mass of bone between them. It is formed of the following: the centrum, parts of the vertebral arches and the facets. All secondary centres unite with the rest of the vertebrae at approximately the age of twenty five.

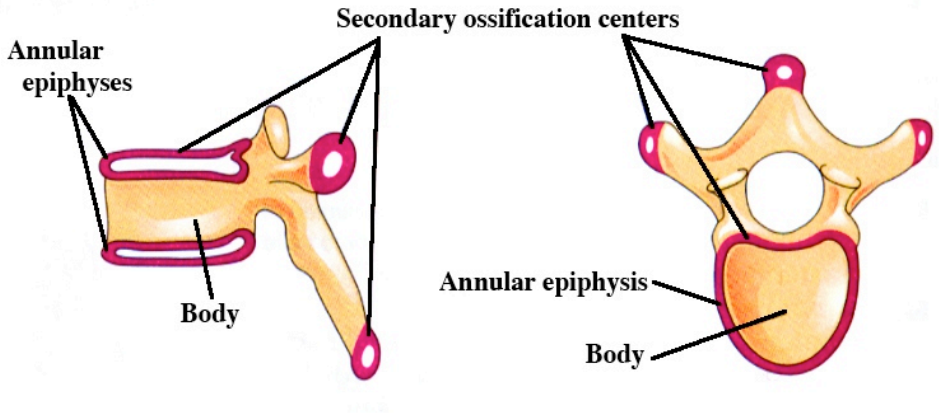

Figure 2.8 The secondary ossification centres. (Adopted from Moore et al., 2008)

2.2 Anatomical Consideration of the Vertebral Column and Intervertebral Discs

The vertebral column is composed of bony vertebrae and fibro-cartilaginous discs connected to each other by the strong ligaments. It is supported by musculature that extends from the skull to the pelvis. Its function is to support the trunk and protect the spinal cord. It lies in the general vertebral plane, which is median and posterior in the body. Its average length in males is 70cm and 60cm in females. Although it is known that the vertebral column is formed of 33 vertebral segments, variations in the numbers are not unusual with the reported variations between 32 to 35 vertebrae, see Figure 2.9 [Terry Canale and Beaty, 2007].

The remainder of this subsection describes the anatomy of the vertebral column, vertebrae and intervertebral discs. In more detail, Section 2.2.1 outlines the general consideration of vertebral

column as a single functional unit. Section 2.2.2 discusses the curvatures of the vertebral column. Section 2.2.3 details the general features of vertebrae. Section 2.2.4 describes the ligaments of the vertebral column. Section 2.2.5 describes the articulations within the vertebral column. Finally, Section 2.2.6 describes the different movements within the vertebral column.

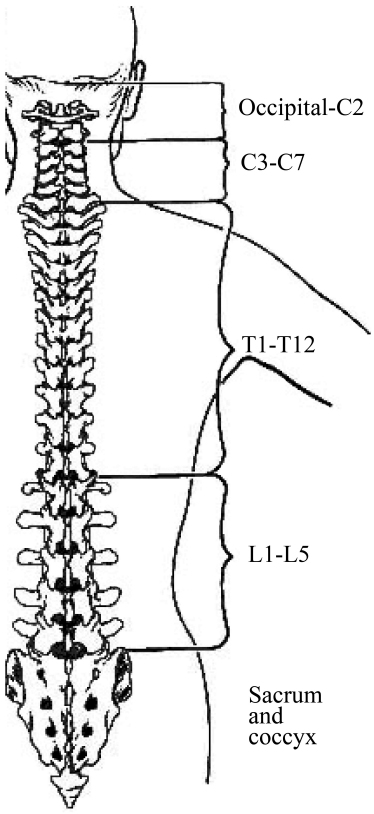

Figure 2.9 Vertebral column formed of alternating 33 vertebrae (7 cervical, 12 thoracic, 5 lumbar, 5 sacral, and 4 coccygeal) and intervertebral discs. (Adopted from Terry Canale and Beaty, 2007)

2.2.1 General Consideration of Vertebral Column as One Functional Unit

Throughout life, the structure, growth and morphology of the vertebral column go through progressive changes. Factors influencing these changes are either external (including mechanical and environmental factors) or internal (including genetic, metabolic and hormonal factors). All these factors determine the vertebral column's ability to meet the dynamic challenges of everyday activities (e.g., traction, compression and shear). External factors are influenced by the occupation, posture and locomotion.

2.2.2 Line of Gravity and Curvatures of the Vertebral Column

The line of gravity is considered as the longitudinal axis that is normally maintained in the erect and well-balanced posture. This line extends caudally from the cranium at the following points:

- Through the external auditory meatus.
- Through the dense of the first vertebra C1.
- Just anterior to the body of the T2.
- Through the centre of T12.
- Through the posterior part of the body of L5.
- Just anterior to the sacrum.

In the coronal plane, a normal vertebral column has no lateral curvatures. This is different from sagittal plane, as multiple curvatures are well demarcated. Curvatures appear as a result of the in-utero foetal movements starting as early as 7 weeks. Soon after birth and as the baby starts holding the head in upright position, spinal curvatures become more pronounced. As a result of the embryo development in flexion, the *primary* thoracic and sacral curves develop as anterior concave curvatures. As the functional muscles develop, they result in the development of the *secondary* cervical and lumbar curvatures. These are known as the lumbar and cervical lordosis as illustrated in Figure 2.10 [Standring et al., 2005]. An infant can support the head at three to four months, acquire an upright sitting posture at about nine months and start walking between twelve to fifteen months. All these functional changes influence the development of the secondary curvatures and change the size of the vertebrae, predominantly in the lumbar region.

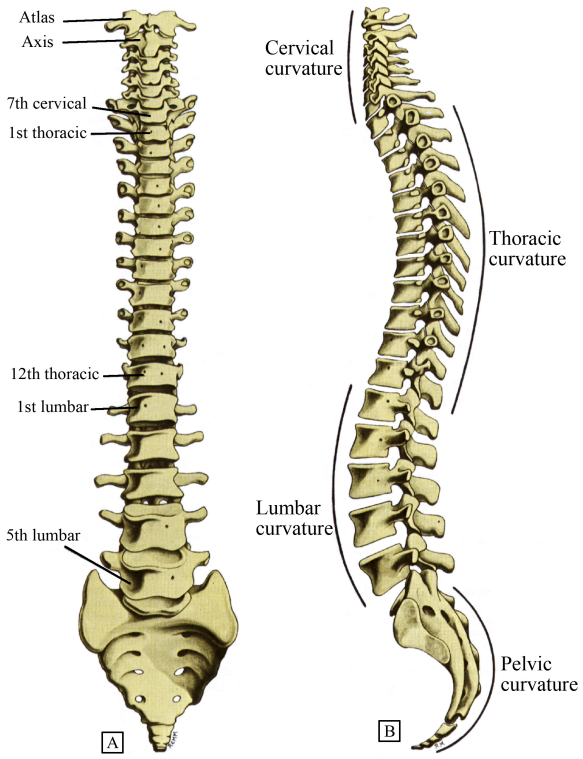

Figure 2.10A The coronal plane, the normal vertebral column shows no lateral curvatures.

Figure 2.10B Thoracic and sacral curves as anteriorly concave curvatures. Cervical and lumbar lordosis. (Reproduced with permission from Standring et al, Gray's anatomy the anatomical basis of clinical practice, 2005)

2.2.3 General Features of Vertebrae

Any typical vertebra is essentially formed of a ventral vertebral body and a dorsal neural arch. Lever-like processes may extend the vertebra. The neural arch and its extensions together enclose the vertebral foramen. The spinal cord, surrounding meninges and blood vessels occupy the vertebral foramen, also known as the neural foramen. The opposed surfaces of adjacent vertebral bodies are bound together by the fibrocartilage intervertebral discs (IVDs). The complete column of vertebral bodies and intervertebral discs form the strong and flexible central axis for the body. The vertebral column also transmits forces to lower limbs due to its muscular attachments. The neural arch and the posterior aspect of each vertebral body form the vertebral canal, through which the spinal cord emerges. See Figure 2.11 [Standring et al., 2005].

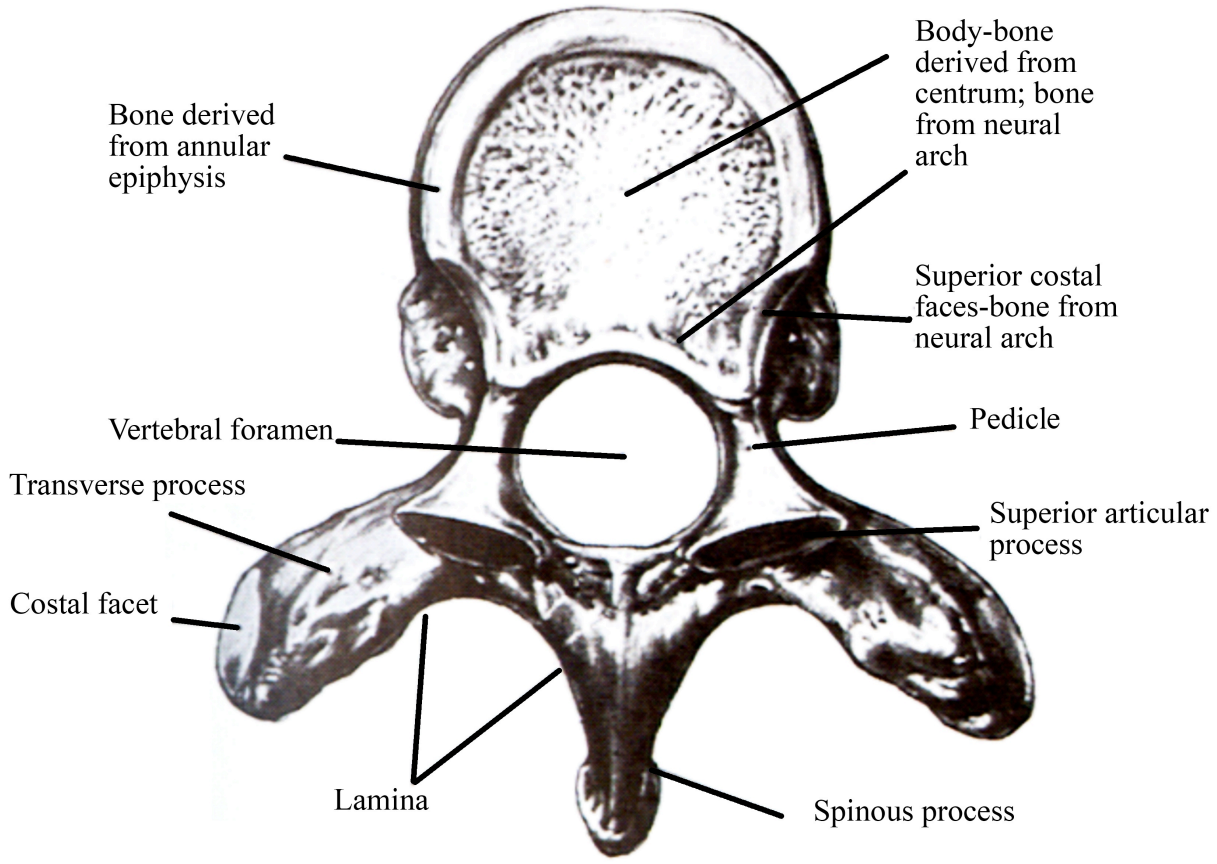

Figure 2.11 Diagrammatic structure of the typical vertebra. (Reproduced with permission from Standring et al, Gray's anatomy the anatomical basis of clinical practice, 2005)

The intervertebral foramina transmit mixed spinal nerves, smaller recurrent nerves and blood and lymphatic vessels. Vertebral bodies normally vary in size, shape and proportion from one spinal level to another. It may even vary within the same region of the vertebral column as is the case in cervical vertebrae. In the horizontal plane, the anterior profile of every vertebral body is convex, and the posterior profile is concave (see Figure 2.11 [Standring et al., 2005]). In the vertical plane, vertebrae are concave anteriorly and flat posteriorly enabling them to complete the vertebral foramen (see Figure 2.12 [Standring et al., 2005]). Small vascular foramina may appear in the front and sides of the vertebral bodies. On the posterior aspect, there are small arterial foramina and one (or possibly two) large irregular orifice(s) for the exit of the basivertbral veins.

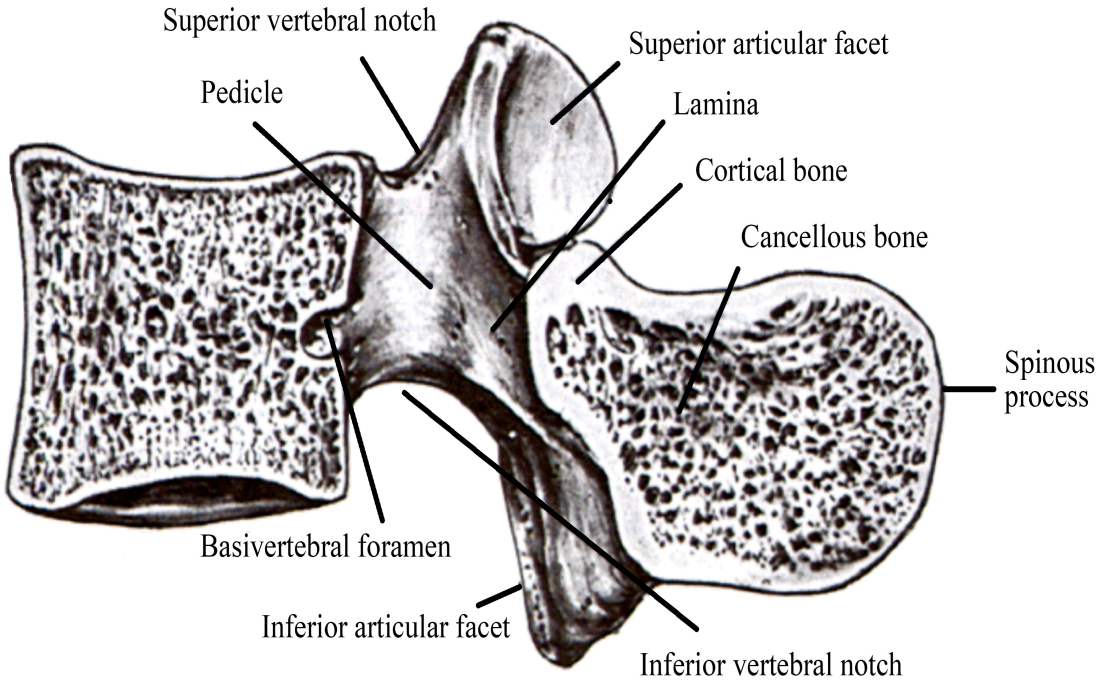

Figure 2.12 The vertical profile of the vertebra. (Reproduced with permission from Standring et al, Gray's anatomy the anatomical basis of clinical practice, 2005)

Each side of the vertebral arch has a vertically narrow ventral part known as the pedicle, and another, dorsally broader part known as the lamina. As indicated by their names, superior and inferior articular processes are projected on the superior and inferior surfaces, respectively. The spinal process is projected posteriorly.

The pedicles are the short, thick and rounded dorsal projections from the superior part of the vertebral body at the junction of its lateral and dorsal surfaces. Each pedicle has a bi-concave border, formed by a shallow concave superior border and a deeper concave inferior border, known as the superior and inferior vertebral notches, respectively (see Figure 2.12 [Standring et al., 2005]). Adjacent intervertebral notches contribute to form the intervertebral foramen when the vertebrae articulate together. The vertebral articulation is achieved by the intervertebral discs and the zygapophyseal joints. The complete perimeter of the intervertebral foramen consists of

the notches, the dorsolateral aspect of the adjacent vertebral bodies, the intervertebral discs and the capsules of synovial zygapophyseal joints.

Laminae are the direct continuation of the pedicles dorsally. They are flat vertically and curved dorsomedialy. Both laminae and the base of the spinous process complete the neural foramen.

The *spinous processes* are projected dorsally and often caudally from the junctions of the laminae. They vary in size, shape and directions. Their main function is to act as levers for the attached muscles which control posture and various active movements. Superior and inferior articular facets (known as zygapophyses) arise at the pediculolaminar junction. The superior process projects cranially, bearing a dorsal facet that has either a lateral or medial inclination (depending on the concerned spinal level). Inferior process bulges caudally with the articular facet which is directed ventrally (again with either medial or lateral inclination according to the spinal level). Articular processes of the adjoining vertebrae form small synovial zygapophyseal joints. These joints permit variable amounts of movement between the vertebrae, depending on the spinal level.

The *transverse processes* project laterally from the junctions between the pedicles and the laminae. They act as levers for the muscles and the ligaments, especially those concerned with rotation and lateral flexion. Thoracic transverse processes also articulate with the ribs.

Each vertebra has internal trabeculae of compact bone forming an external shell, which is perforated at the vascular foramina. This shell is thin in the discal surface but thicker in the arches and the projections. All vertebrae from the second cervical vertebra (C2) down to the first sacral (S1) vertebra articulate by the following: (1) cartilaginous joints between the vertebral bodies, (2) synovial joints between the vertebral processes, and (3) fibrous joints between the vertebral laminae and also between the vertebral transverse processes and spinous processes.

2.2.4 Ligaments of the Vertebral Column

Fibrocartilagenous intervertebral discs and lamina are connected by hyaline cartilages, all together form the symphyses. Vertebral bodies are united together by the anterior and posterior longitudinal ligaments. The anterior longitudinal ligament is a strong band extending on the anterior surface of the vertebral bodies. It is broad on the caudal end. It is also thick and narrow in the thoracic region compared to both the cervical and lumbar regions. It is relatively thick and narrow opposite vertebral bodies compared to the levels of the intervertebral symphyses. The anterior longitudinal ligament is attached to the basilar occipital bone. It extends to the anterior tubercle of C1 (Atlas) and the front of the body of C2 (Axis), and continue caudally to the front of the upper sacrum. It has longitudinally arranged fibers that are strongly attached to the intervertebral discs, end plates and margins of the adjacent vertebral bodies. They are loosely attached to the intermediate level of the vertebral bodies. The ligament fills the anterior concavities of the vertebral bodies, thus flattening the anterior profile of the vertebral column (see Figure 2.13 [Standring et al., 2005]). At various levels, the ligamentous fibers blend with the adjacent periosteum, perichondrium and periphery of the annulus fibrosus. It has several layers, the most superficial fibers being longest as they extend over three or four vertebrae. Intermediate fibers, on the other hand, extend over two to three bodies, while the deepest fibers extend from one vertebral body to the next.

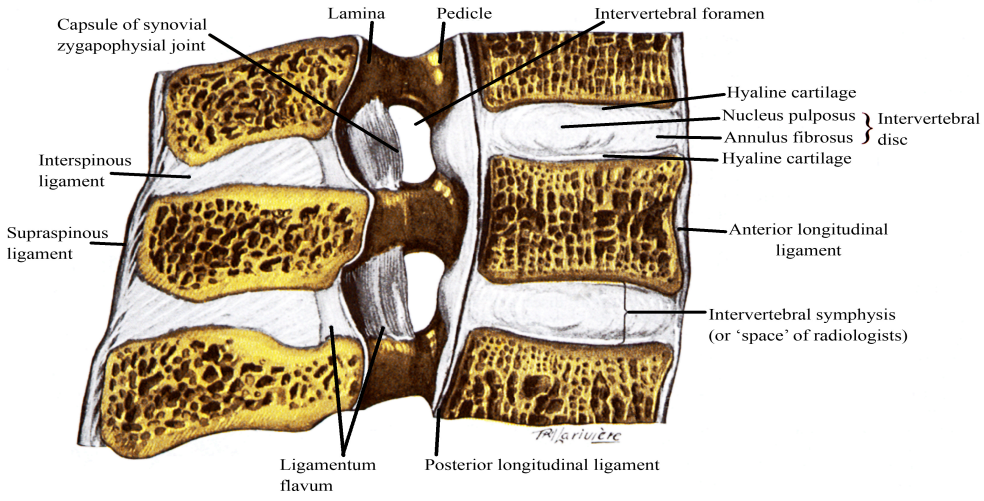

Figure 2.13 The ligaments of the vertebral column. (Reproduced with permission from Standring et al, Gray's anatomy the anatomical basis of clinical practice, 2005)

The posterior longitudinal ligament extends on the posterior surface of the vertebral bodies and within the vertebral canal. It is attached to the body of C2 down to the sacrum. It has smooth glistening fibers attached to the intervertebral discs, end plates and margins of the vertebral bodies. At the cervical and upper thoracic bodies, the ligament is broad and of uniform width. However, at the rest of the thoracic and lumbar region it is narrow over the vertebral bodies and broad over the discs, as illustrated in Figure 2.14 [Standring et al., 2005].

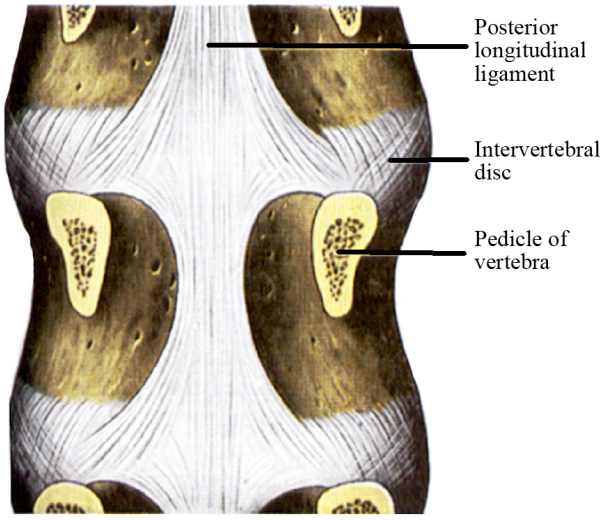

Figure 2.14 The posterior longitudinal ligament in the lumbar region. (Reproduced with permission from Standring et al, Gray's anatomy the anatomical basis of clinical practice, 2005)

Fibers of the superficial layer of the posterior longitudinal ligament bridge three to four vertebrae. The deeper layer connects two adjacent vertebrae as the peri-vertebral ligaments. This deep layer is close to, and fused with, the annulus fibrosus of the intervertebral discs. Layers of the posterior longitudinal ligament are more distinct in the immediate postnatal life.

2.2.5 Joints of the Vertebral Column

Joints between the vertebral articular processes vary in shape from one vertebral level to another. These synovial joints are known as the *Zygapophyseal joints*. Laminae, spines and transverse processes of the vertebrae are connected through syndesmoses. *Ligamentum flava*, *interspinous*,

supraspinous, *intertransverse ligaments* and *ligamentum nuchae* form these syndesmoses. While some authors may classify these ligaments as accessory ligaments to the zygapophyseal joints, others classify them as a separate anatomical identity known as syndesmoses. In what follows, we discuss those two structures in more detail.

The *Zygapophyseal Joints* are variable joints; they are either simple synovial joints (the cervical and thoracic spine Zygapophyses joints), or complex synovial joints (as is the case in the lumbar spine). The articular processes of the opposed vertebrae carry the articular surfaces of superior and inferior articular facets, see Figure 2.15 [Standring et al., 2005]. Each facet is covered by hyaline cartilage. Their sizes, shape and orientation vary from one spinal level to another. The Zygapophyseal joints have thin capsules which are loosely attached to the margins of the articular facets. They are longer and looser in the cervical regions.

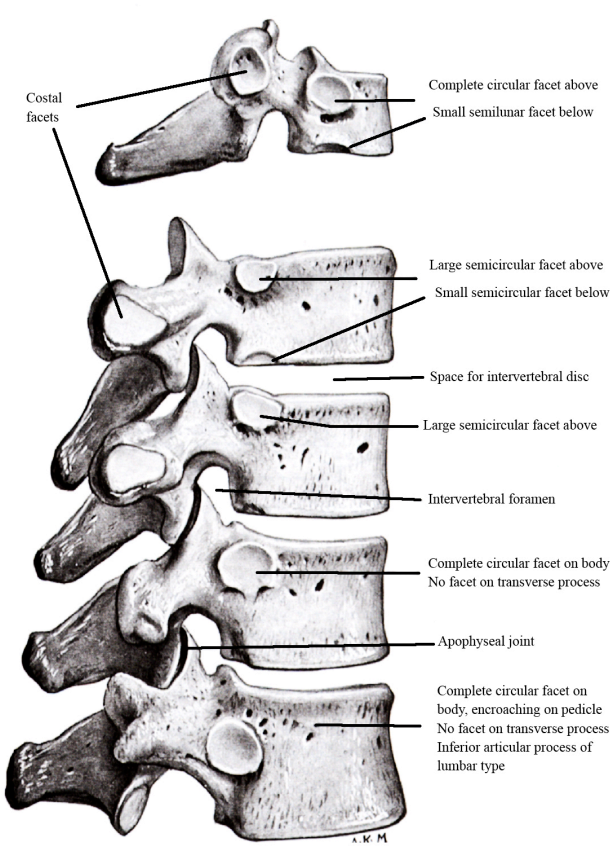

Figure 2.15 Articulations between adjacent vertebrae to form the vertebral column as one unit. (Reproduced with permission from Standring et al, Gray's anatomy the anatomical basis of clinical practice, 2005)

The *Intervertebral Syndesmoses* consist of the following structures:

- The ligamentum flavum connects the laminae of adjacent vertebrae within the vertebral canal, see Figure 2.16 [Standring et al., 2005]. Its attachment extends from the zygapophyseal capsules to the point where both laminae fuse to form the spinous process. The posterior margins of the ligamentum flavum are partially united, leaving intervals to provide space for the vertebral venous plexuses. The ligamentum flavum is predominantly formed of yellow elastic tissues, hence its name (flavum means yellow in Latin). Fibers of the ligamentum flavum are almost perpendicular descending from the lower anterior surface of one lamina to the posterior surface of the lamina below. In the cervical spine, the ligament is thin, broad and has long fibers. It is thick in the thoracic spine, and even thicker in the lumbar area. Its main function is to arrest separation of the laminae in spinal flexion, thus preventing abrupt movements. It also helps in restoring erect posture after flexion, thus protecting discs from injury.

- Supra spinous ligament is the strong fibrous cord connecting the tips of the spinous processes from C7 to the sacrum. It is thick and broad at the lumbar levels and is intimately blended with the neighbouring fascia. Its most superficial layer extends over three to four vertebrae, the deeper layer spans two to three vertebrae, and the deepest layer only connects the adjacent vertebrae. Between the spines of C7 and the external occipital protuberance, the supraspinous ligament is replaced with the ligamentum nuchae.

- Ligamentum Nuchae is the bi-laminar fibroelastic intermuscular septum. It acts as a septum for the bilateral attachment of the cervical muscles and their sheaths. It is often considered as being homologous with (but structurally separate from) the supra spinous and interspinous ligaments in the neck. It has dense bilateral fibroelastic laminae; a layer of areolar tissue separates both layers. Both laminae are blended at its posterior free border. These fibroelastic laminae are attached to the median part of the external occipital crest, the posterior tubercle of C1 and the medial aspect of the bifid spines of remaining cervical vertebrae (C2-C7).

- Interspinous ligaments are thin and almost membranous ligaments connecting the adjoining spinous processes. They extend from the root to the apex of each spinous process meeting with the ligamentum flavum. They are narrow and elongated in the thoracic region, but broad and thick in the lumbar region. Interspinous ligaments are poorly developed in the cervical spine.

- Intertransverse ligaments are found between the transverse processes. At the cervical spine they consist of few and irregular fibers that are largely replaced by inter transverse muscles. However, in the thoracic region they are cords intimately blended with adjacent muscles. In the lumbar area they are thin and membranous.

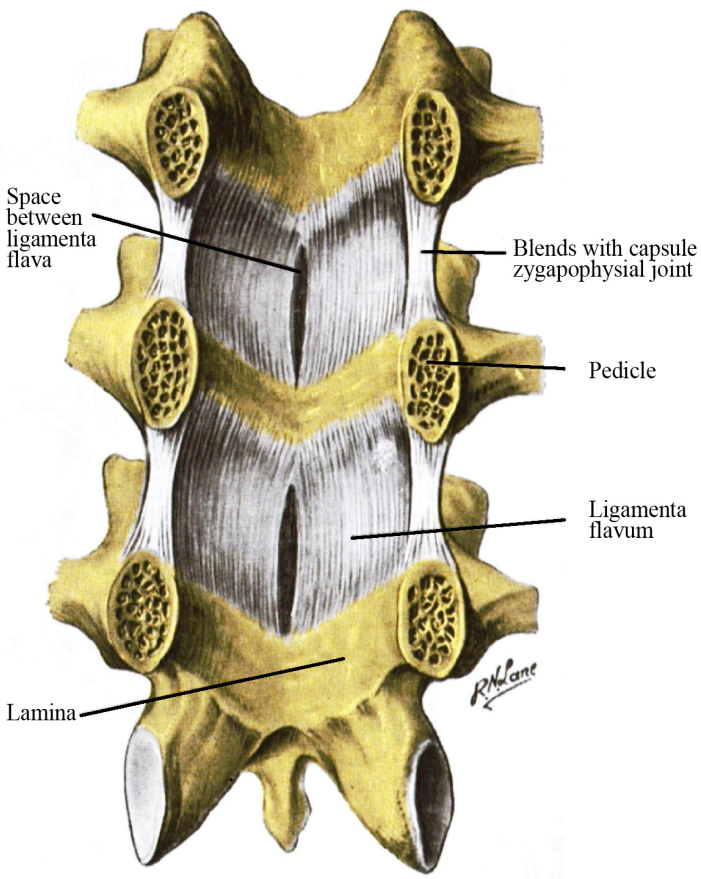

Figure 2.16 The ligamentum Flavum. (Reproduced with permission from Standring et al, Gray's anatomy the anatomical basis of clinical practice, 2005)

2.2.6 Vertebral Column Movements

The intervertebral discs allow for movements between the vertebrae. These movements are restricted by the orientation of the zygapophyseal joints. Although there are limited movements between individual vertebrae, the summation gives large total range of flexion, extension, lateral bending, rotation and circumduction in the vertebral column. These are described in more detail below:

- *Flexion:* In flexion the anterior parts of the intervertebral discs are compressed, resulting in relaxed anterior longitudinal ligament. The following posterior components of the vertebral column are all tense: (1) the interspinous ligaments, (2) the supraspinous ligaments, (3) the posterior fibers of the intervertebral discs, and (4) the posterior longitudinal ligament. As a result of flexion, the interlaminar intervals expand. Furthermore, the gliding movement of the inferior articular processes on the superior processes of the adjacent vertebrae result in tightening the capsules of the zygapophyseal joints.

- *Extension:* The events that occur during extension are opposite to those occurring during flexion. Extension is limited by the tension in the anterior longitudinal ligament, the anterior discal fibers and the zygapophyseal joints. Approximation of the spinous processes is another limiting factor. Both the cervical and lumbar vertebrae allow for a wide range of extension. It is however limited in the thoracic vertebrae due to the thoracic cage skeleton, the muscles and the relatively thinner intervertebral discs.

- *Lateral flexion and Rotation*: Lateral flexion is often combined with rotation. During lateral flexion and rotation, the intervertebral discs are laterally compressed, contra-laterally tensed and lengthened. The lateral flexion is wider in the cervical and lumbar vertebrae. During the rotation of the vertebral column, the twisting of the vertebrae is associated with torsion deformation of the intervertebral discs.

2.3 The Intervertebral Discs

This subsection describes the three component of the intervertebral disc, namely, the nucleus pulposus, the annulus fibrosus, and the cartilage end plate.

2.3.1 Structure of the Nucleus Pulposus

The clear gelatinous material of the Nucleus Pulposus [NP] occupies 50% of the IVD [Mirza and White. 1995]. More specifically, the nucleus pulposus is formed of a randomly organized network of collagen fibers and radially arranged elastin fibers. The elastin fibers are embedded in a highly hydrated aggrecan-containing gel and the chondrocyte-like cells that are interspersed at a low density (approximately 5000/mm^3). Outside the nucleus pulposus is the annulus fibrosus, and the boundary separating the two is very distinct in the young healthy discs [Prithvi-Raj, 2008]. The nucleus pulposus has a relatively high pressure that precludes any vascular supply and also could explain why the nucleus pulposus contains no nerves or nerve endings [Jeffcoate, 1977].

The nucleus pulposus is typically located in an eccentric position within the intervertebral disc space, as it is usually closer to the posterior margin of the annulus. [Parke and Schiff, 1971]. The nucleus pulposus moves within the disc space as the posture changes. Frequently, the nucleus pulposus communicates with the epidural space and the surrounding neural structures [Mirza and White, 1995]. It mostly contains water that is retained by the physicochemical properties of the colloid gel. To be more precise, it is retained by the affinity of the protein-polysaccharide complexes to retain water. Discs may be punctured with relative impunity [Hendry, 1958]. In normal healthy individuals, the semifluid consistency of the nucleus pulposus enables it to transmit compressive forces evenly in all directions. This capacity is known as "isotropic incompressibility" [Jeffcoate, 1977].

2.3.2 Structure of the Annulus Fibrosus

The annulus fibrosus consists of a series of fibrous lamellae that encloses the nucleus pulposus. It strongly unites the vertebral bodies. Its main role is to withstand any tension generated by one of the following: the tensile forces from the horizontal expansion of the compressed nucleus, the torsional stresses of the vertebral column, or the separation of the vertebral bodies on the convex side of the spinal flexures. On macroscopic dissection, the lamella encircling the discs are composed of glistening fibers running obliquely and spirally in relation to the axis of the vertebral column [Parke and Schiff, 1971]. These are made up of a series of 15 to 25 concentric rings, or lamellae, arranged in criss-cross pattern. Each layer is 0.14-0.52 mm thick. These layers are relatively thicker in the lateral portion of the annulus and the inner layer of the annulus. The total disc height contains 20-62 bundles of collagen fibers [Mirza and White, 1995]. These fibers lie parallel within each lamella. The fibers are oriented at approximately 60° to the vertical axis, alternating in medial or lateral direction. Elastin fibers lie between these lamellae to help the disc return to its original arrangement following bending, flexion or extension. Elastin fibers also bind the lamellae together since they pass radially from one lamella to the next. Cells of the annulus, particularly in the outer region, have fibroblast-like characters; they are elongated, thin, and aligned parallel to the collagen fibers. Towards the inner part of the annulus, these cells are more oval. Cells of both components of the disc (i.e., the annulus and nucleus) have several long, thin cytoplasmic projections, which may be more than 30 micrometre long each. Such features are not seen in cells of other articular cartilages. Their function in the disc remains unknown to day, but it has been suggested that they may act as sensors and communicators of mechanical strain within the tissue [Prithvi Raj, 2008].

2.3.3 Structure of the Cartilaginous Endplate (CEP)

The third morphologically distinct structure in the intervertebral disc is the cartilage endplate. It is a thin horizontal layer, usually less than 1 mm thick, of hyaline cartilage. Its main function is interfacing the disc and the vertebral body. The collagen fibers within the cartilage end plate run horizontal and parallel to the vertebral bodies, with the fibers continuing into the disc. See Figure 2.17 [Prithvi-Raj, 2008].

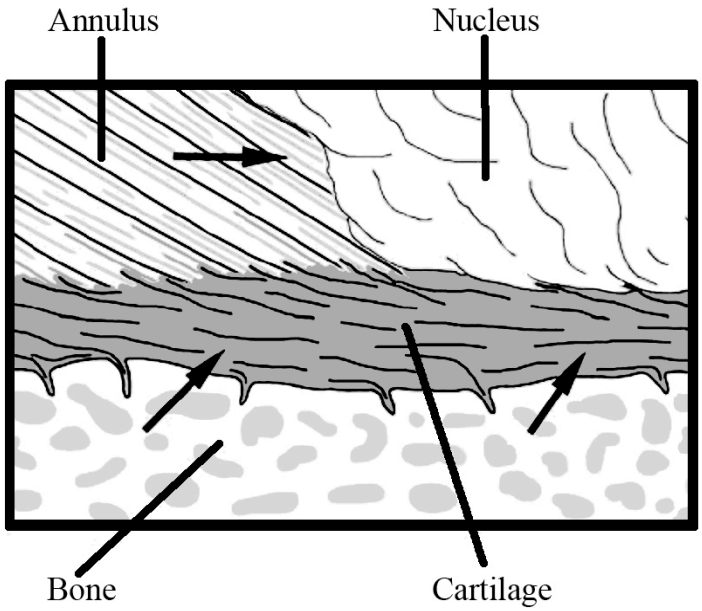

Figure 2.17 The organization of the vertebral endplate containing hyaline cartilage bonded to the perforated cortical bone of the vertebral body and collagen fibers of the annulus and the nucleus. Arrows indicate routes for nutrient transport from blood vessels into the central portion of the disc. (Adopted from Prithvi-Raj, 2008)

2.3.4 Vascular Supply of the Intervertebral Disc

Blood vessels surrounding the intervertebral discs during early development phases will eventually disappear. Subsequently, the resulting tissue will be totally avascular disc material. Most of the mature disc nutrients will be carried out by diffusion to and from the highly vascular cancellous bone of the adjacent vertebral body [Humzah and Soames, 1988].

Smith and Walmsley [1951] suggested exceptions from being totally avascular. In more detail, by studying rabbits' spinal models, they concluded that the most peripheral parts of the intervertebral discs receive some blood supply from its adjacent blood vessels. They also suggested that the vascular and avascular parts of the mature discs are different in their reaction to injury [Smith and Walmsley, 1951]. In 1984, Crock and Goldwasser examined the circulation at the region of the CEP in Dogs (greyhounds in particular). They also observed a bed of capillaries over the bone-disc interface that is dense in areas related to the NP [Crock and

Goldwasser, 1984]. More recently, it has been suggested that adult discs show very few blood vessels within their tissue [Prithvi-Raj, 2008].

The Cartilage End Plate (CEP), like any other hyaline cartilage, is totally avascular and aneural. However, blood vessels are present in the longitudinal ligaments adjacent to intervertebral discs. Moreover, in infantile cartilage endplates (i.e., during the first 12 months since birth), nutrient vessels do branch from the corresponding spinal artery (see Figure 2.18 [Prithvi-Raj, 2008]).

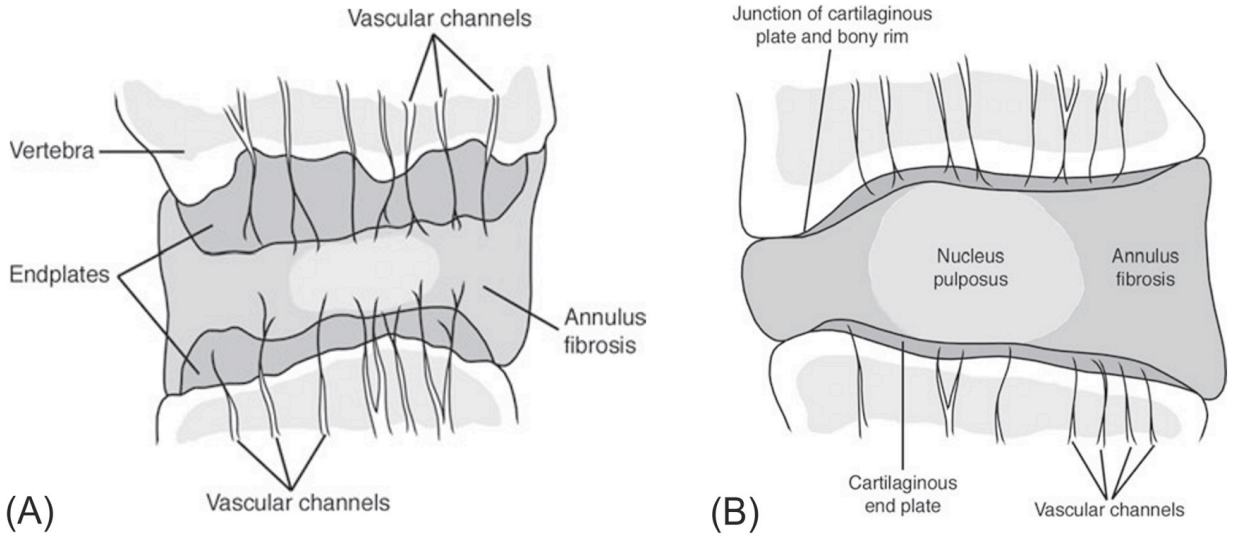

Figure. 2.18 (A) An axial section of the intervertebral disc in a 10-month-old girl. Observe the numerous vascular channels and wide cartilaginous endplates traversing to the annulus fibrosis and Nucleus Pulposus. The disc is more gel-like and highly hydrated. (B) An axial section of the intervertebral disc of a 50-year-old adult. Note the thin cartilaginous plate and lesser vascular channels traversing to less hydrated distinct Annulus Fibrosis and Nucleus Pulposus. (Adopted from Prithvi-Raj, 2008)

2.3.5 Nerve Supply of the Intervertebral Discs

The sinuvertebral nerves, also known as the *"ramus meningeus"* or *"the recurrent sinovertebral nerve"* are recurrent nerves within the vertebral canal. They supply all the fibrous connective tissue within the spinal canal, including the posterior longitudinal ligament, periosteum, venous sinuses and the dural layers of the same level. These nerves are considered to be equivalent to the recurrent meningeal branches of cranial nerves [Humzah and Soames, 1988].

Many authors contributed to the understandings of the intervertebral disc nerve supply [Roofe, 1940; Pedersen et al., 1956]. They described two origins of the sinuvertebral nerves as follow:

- *The spinal root:* it originates directly from the spinal nerve that is distal to the dorsal root ganglion. It then re-enters the spinal canal to reach the midline. The spinal root gives direct branches to both discs above and below each level (See Figure 2.19 and Figure 2.20) [Prithvi-Raj, 2008].
- *The sympathetic root:* it originates from the sympathetic nervous system. This explains its vascular association.

The sinuvertebral nerves exit from the dorsal root ganglion and enters the foramen. It divides into two nerves: the major ascending root, and the lesser descending branch.

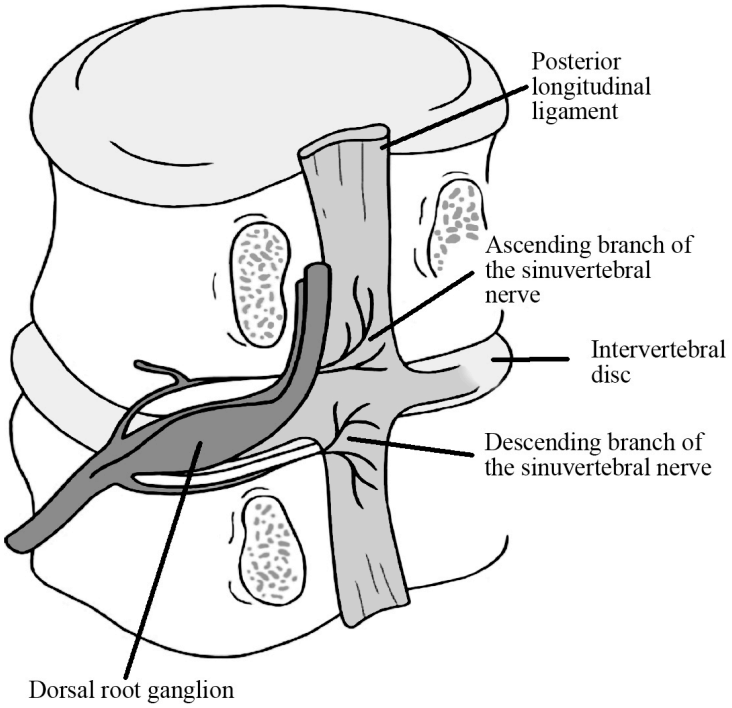

Figure. 2.19 Innervation of the PLL and the disc annulus by the ascending branch of the Sino-vertebral nerve. (Adopted from Prithvi-Raj, 2008)

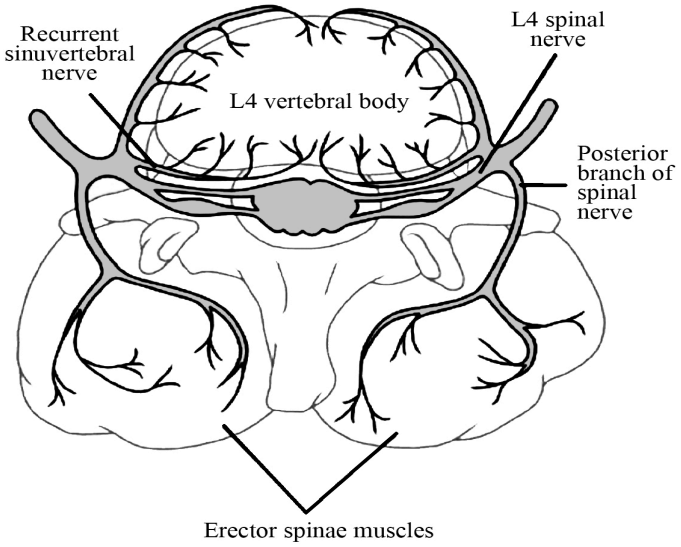

Figure 2.20 Course of the recurrent Sinuvertebral nerve. The nerve exits from the dorsal root ganglion and enters the vertebral foramen, it divides into a major ascending and a lesser descending branch. PLL is richly innervated by fibers from the ascending branch of the Sinuvertebral nerve. (Adopted from Prithvi-Raj, 2008)

Roofe [1940] and Stilwell [1956] both confirmed the presence of fine un-myelinated nerve fibers at the attachment of the posterior longitudinal ligament to the posterior aspect of the annulus. However none were found within the annulus itself. Malinsky [1959] found complex nerve endings as well as nerve receptors (both encapsulated and nonencapsulated receptors) within the posterior longitudinal ligament, anterior longitudinal ligament, and superficial layers of the annulus fibrosus.

Nerve supply and nerve distribution in the foetal and adult intervertebral discs were studied by Serrano Vela [1973]. Numerous fine nerve filaments were identified within the anterior longitudinal ligament and posterior longitudinal ligament. Nerve filaments were also identifed within the outermost 1-2mm of the annulus fibrosus and within the connective tissue separating the posterior longitudinal ligament from the lamellae of the annulus fibrosus. However, no nerve fibers were identified within the central zone of the adult IVD. Serrano Vela implied that the innervations to the disc are not only via the sinuvertebral nerve, but also via the anterior fibers that are unmyelinated [Bogduk et al., 1981]. The close relation between the intervertebral disc and the spinal nerve roots is responsible for the pathological consequences of disc displacement.

2.4 Reported Research for the Intervertebral Disc Pressure Measurement.

Petter [1933] observed an outward bulging of any sectioned cut surface of the intervertebral discs while dissecting disc specimens. An observation led to the following conclusion:

"In addition to the superincumbent weight and ligamentous pull which act as an external force on each disc, there also exists an internal expansive force from within the disc".

Petter, 1933

In the basic study, Petter [1933] examined post mortem spinal specimens collected from tuberculosis patients. He aimed to collect these specimens within a maximum of four hours after death to maximize the accuracy of his study. He also observed that in a block of two or more vertebral bodies, the intervening discs become longer when it is removed from the body. This observation was based on the increased distances between marker pegs inserted into each vertebral body (See Figure 2.21) [Petter,1933].

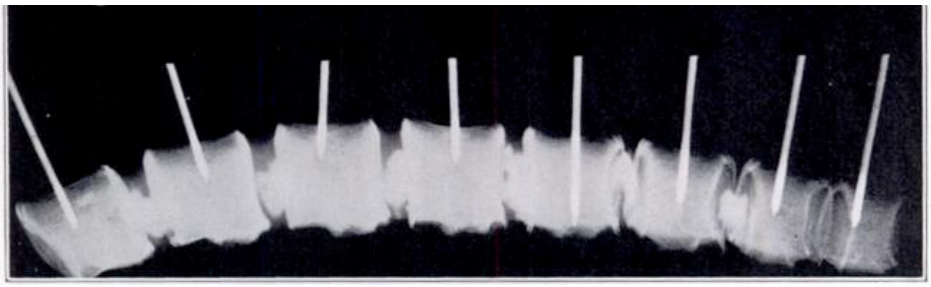

Figure 2.21 The marker pegs inserted into each vertebral body. (Petter, 1933)

The distance between these markers pegs was measured while the specimens remained in-situ; this distance was denoted as "S". The distance between the same markers was measured again when the specimen was removed from the deceased body; he denoted this distance as "R". Further release of the annulus fibrosis of each disc throughout its entire circumference was done

so that the restricting forces were released. After that, the distance between the markers was measured again, this time denoted as “CC”. Constant increase in the distances was observed when comparing distances “S”, “R” and “CC”. See Figure 2.22 [Petter,1933].

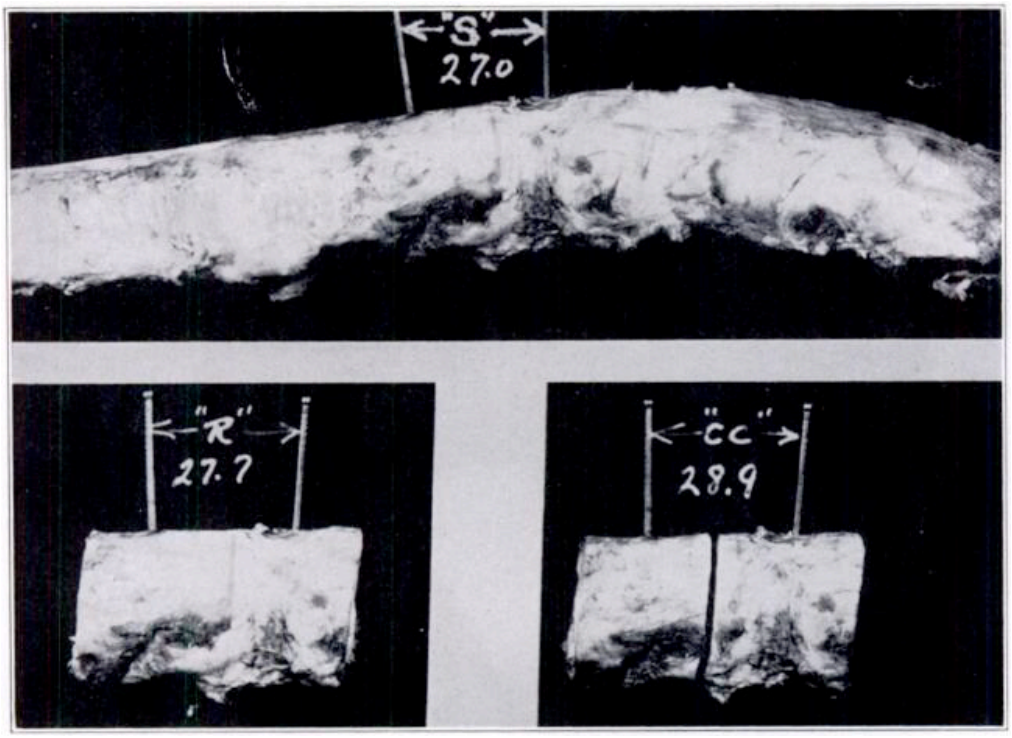

Figure 2.22 Constant increases in the distances were observed when comparing “S”, “R” and “CC” (Petter, 1933).

In an attempt to measure “the expansible force within the intervertebral disc”, also referred to as “pressure within intervertebral disc” in that same study, Petter [1933] assumed that the force required to reduce the distance “CC” to “R” is equal to “the pressure within intervertebral disc”. The pressure within the intervertebral discs was recorded to be constant between 30 and 32 pounds. In the early 1950s, Nachemson [1959] studied the intervertebral disc pressure measurement in a more detailed and scientific approach. His studies were done using an in-vitro spinal motion segment models placed vertically in a pneumatic clamp. See Figure 2.23, taken from [Nachemson 1959].

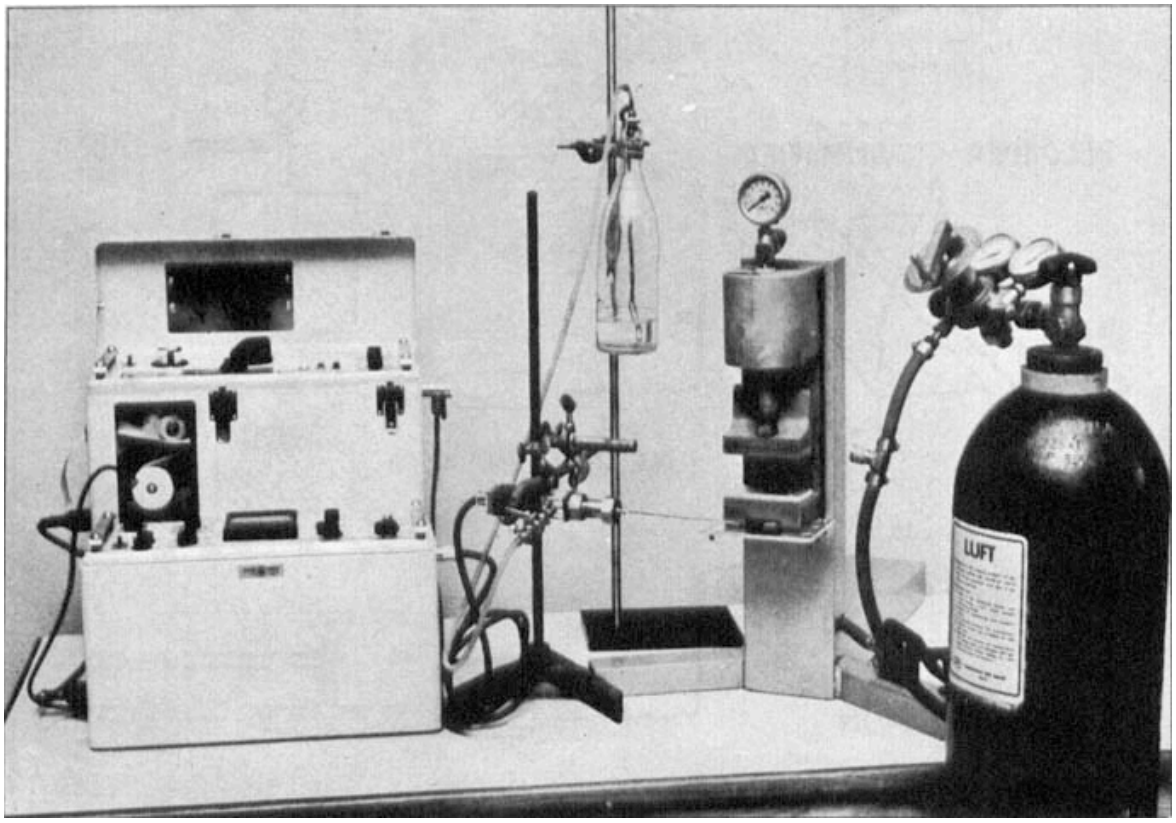

Figure 2.23 Vertebral bodies with intervertebral discs vertically placed in a pneumatic clamp (Nachemson, 1959).

Each specimen was formed of two adjacent vertebral bodies with the intervertebral disc in-between. Laminectomy was performed for all specimens allowing easy access to the intervertebral discs. In total, thirty-seven specimens were collected. Specimens were grouped into two main categories; 11 specimens labelled to be “normal” while the remaining 26 specimens were labelled “degenerated”. The degenerated group included any specimens showing macroscopic annular rupture or macroscopic damage to the nucleus pulposus on gross anatomical examination. Nachemson attached a Leur-Lok needle to a polyethylene tubing system filled with distilled water. The needle was inserted into the disc by passing it through graded cannula to determine the depth of the needle. See Figure 2.24 [Nachemson 1959].

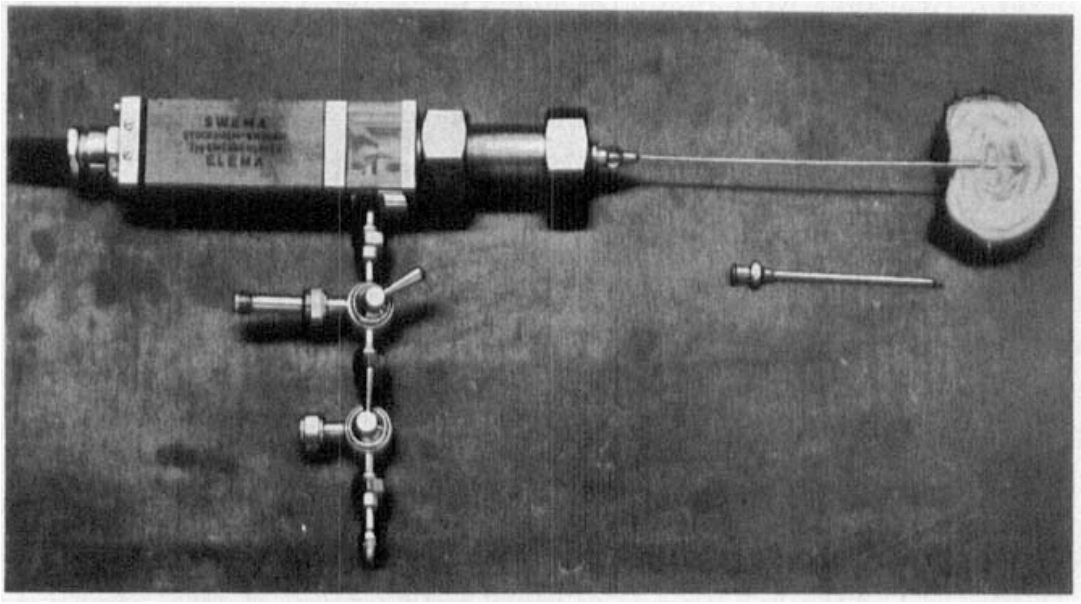

Figure 2.24 The needle and plastic tubing. Its position is demonstrated on a cross-sectioned disc. (Nachemson, 1959)

To confirm the needle did not change its shape or position within the disc space, two planes Roentgen were taken prior to any testing. See Figure 2.25 [Nachemson 1959].

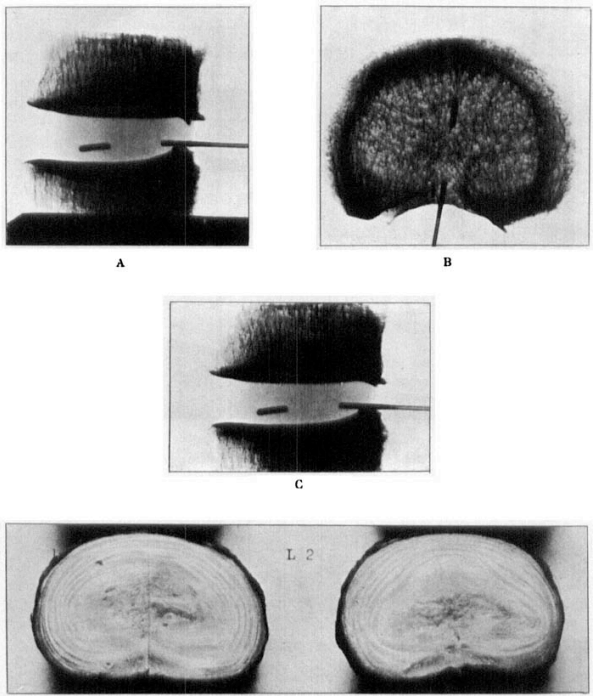

Figure 2.25 Roentgen plates and macroscopic appearance of a normal disc. (Adopted from Nachemson, 1959)

Needle with its attached plastic catheter was connected to a mechano-electrical pressure transducer. This transducer was built on the strain-gauge principle. To avoid invalidating the result, any air bubbles within the system was carefully searched for and promptly evacuated prior to conducting the experiments. Pressure transducer was connected to an amplifier. Values measured were recorded using a writing jet-recorder (mingo-graph) running on a high-speed rotating paper drum. In order to achieve a clear idea about the intervertebral disc pressure as well as to be able to compare results, the surface area for each studied disc was determined using an Amsler planimeter. See Figure 2.26 [Nachemson 1959].

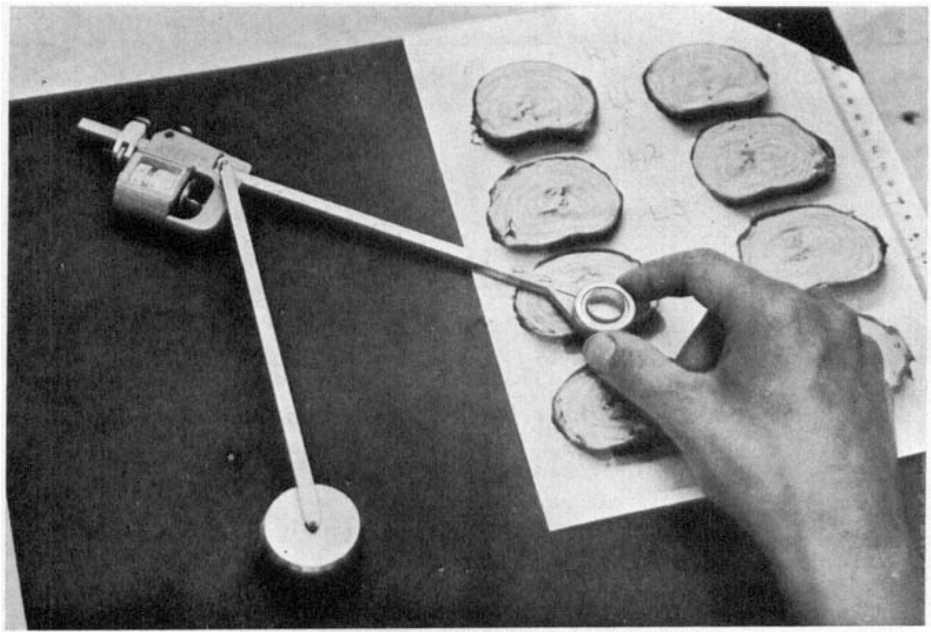

Figure 2.26 Amsler planimeter used to measure the surface area for the studied disc (Nachemson, 1959).

By measuring the intervertebral discs' surface area, Nachemson was able to calculate the intra discal *pressure index*. Using the pressure index, he was able to compare results obtained from different experiments and using different discs. Nachemson [1959] concluded from his experiment that the average values of intervertebral disc pressure are lower for all degenerated discs, i.e. those discs with annulus ruptures and gross anatomical nuclear changes. Nachemson tested discs from L1 to L4. The greatest variations in pressure indices between normal and degenerated discs were found at the L4 level.

Nachemson [1959] concluded the following:

- The weight bearing capacity of the nucleus of a normal L4 disc is 50% more than that of a degenerated one.
- Endplate damage causes 30-40% reduction in the intervertebral disc pressure.
- In degenerated intervertebral discs, the nucleus loses part of its weight-bearing capacity, resulting in more strain on the annulus fibrosus.

Nachemson and Morris [1964] studied the intervertebral disc pressure in-vivo. They conducted experiments using a specially constructed needle equipped with a pressure-sensitive polyethylene membrane. The needle was connected to an electro-manometer designed to record the pressure readings. In this study, discography was performed for all examined discs prior to measuring the disc pressure. Under local anaesthetics, the discography needle was passed through a larger diameter cannula, which was inserted into the nucleus pulposus. In all cases, the disc pressure measurements were taken with the patients sitting upright unsupported with arms hanging at the sides. Ten patients were asked to hold 4.6 kg weights in each hand followed by 11.35 kg (i.e., a total of 9.2 kg first, and 22.5 kg later). Eleven patients were asked to perform Valsalva manoeuvre. Six patients were asked to stand, while fourteen patients were asked to recline on the examination table. Changes in the intervertebral disc pressure due to wearing inflatable corset while standing were studied in four patients. To be able to compare the results, Nachemson and Morris [1964] calculated the cross-sectional surface area of the examined discs using roentgenograms in two planes at right angle to each other. They also considered the load applied on each particular disc used for their study. Therefore, it was essential to evaluate the weight above the used level. For this study, 57% of the body weight was calculated to be above the third lumbar disc, 59% for the fourth lumbar vertebral disc. These data were taken from Ruff [Ruff S: Brief Acceleration: Less than One Second. In German Aviation Medicine, World War II. 1950. Vol. I; pp 584-579. Prepared under the auspices of the Surgeon General, US Air Force].

While analysing the intervertebral disc pressure measurements in normal discs with no additional loading, Nachemson and Morris [1964] demonstrated a clear correlation between the pressure

values for each intervertebral disc level and the body weight above the level concerned, see figures 2.27 and 2.28 [Nachemson and Morris,1964].

RESULTS OBTAINED WITH SUBJECTS IN THE SITTING POSITION, NORMAL DISCS
(Kilograms per Square Centimeter)

Case No.	Disc	A_d Cm.2	W_{part} Kg.	p_n	p	P_{tot}	+9.1 Kilograms p_n	+9.1 Kilograms p	+9.1 Kilograms P_{tot}	+22.7 Kilograms p_n	+22.7 Kilograms p	+22.7 Kilograms P_{tot}	Valsalva Maneuver p_n	Valsalva Maneuver P_{tot}	Valsalva Maneuver p_n Increase (*Per cent*)
1	L-3	16.4	30.8	11.3	7.5	123.0							14.9	162.4	32
2	L-3	18.4	36.3	12.1	8.1	149.0									
3	L-3	18.0	49.1	14.6	9.7	174.6							17.0	203.4	16
4	L-3	13.3	26.0	10.4	6.9	91.8	15.3	10.2	135.7	23.2	15.5	206.2	12.5	110.4	20
5	L-3	17.1	40.2	11.6	7.7	131.7									
	L-4*	19.1	41.6	8.2	5.5	105.1	10.0	6.7	128.0	11.4	7.6	145.2			
7	L-3	17.4	33.3	12.0	8.0	139.2									
8	L-4	17.8	39.2	11.8	7.9	140.6	16.9	11.3	201.1	22.4	14.9	265.2	12.3	146.0	4
10	L-4	14.9	34.9	14.9	9.9	147.5									
11	L-4†	14.9	34.4	7.7	5.1	76.0	11.3	7.5	111.8	19.4	12.9	192.2			
12	L-3	12.1	25.4	11.8	7.9	95.6							12.7	102.9	8
	L-4	14.1	26.3	12.0	8.0	112.8									
13	L-3	11.7	34.7	14.5	9.7	113.5	17.3	11.5	134.6	20.8	13.9	162.6	17.0	132.2	17
15	L-3	19.9	47.5	11.8	7.9	157.2	14.2	9.5	189.1	18.2	12.1	240.8	15.8	209.0	34
16	L-4	21.6	44.4	9.9	6.6	142.6	12.7	8.5	183.6	17.1	11.4	246.2	13.2	190.1	33
17	L-3	13.8	43.3	15.3	10.2	140.8	16.5	11.0	151.8	21.1	14.1	194.6	15.5	142.1	1
18	L-3	15.7	36.5	13.7	9.1	142.9	15.3	10.2	160.1	19.4	12.9	202.5	14.6	152.3	7
19	L-3	20.6	53.2	13.0	8.7	179.2	14.4	9.6	197.8	18.3	12.2	251 3	13 0	179 2	0

Figure 2.27 Pressure values for each intervertebral disc level and the body weight above the level concerned. (Nachemson and Morris,1964)

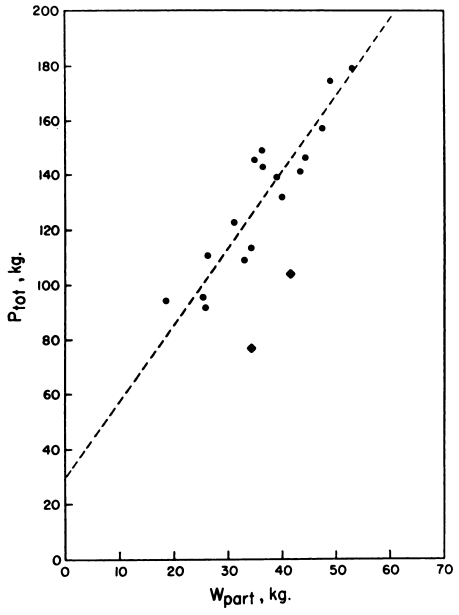

Figure 2.28 Relation between total load on normal disc and calculated part of body weight above that level (sitting position). The Slope determined by means of regression. (Nachemson and Morris, 1964)

While analysing the results in ten normal discs with loads added as the volunteers were asked to carry 9.1 kg and 22.7 kg, Nachemson and Morris observed that additional loads caused a corresponding increase in the total load of the corresponding level. Nachemson also studied the intervertebral disc pressure while volunteers were asked to perform Valsalva manoeuvre, in which case an increase in pressure values was observed in almost all cases.

Recent studies by Sato et al. [1999] involved taking in-vivo measurements of the intervertebral disc pressures in different postures for both healthy individuals and patients with on-going low back problems. In more detail, eight individuals with no history of previous or on-going back problems volunteered for the study. The mean age for this group was 25 years (range 22–29 years). The mean body weight was 73 kg (range 60–96 kg), and mean height was 174cm (range 166–181 cm). An MRI study of the lumbar intervertebral discs was performed before the measurement, confirming normal disc structure in each of the volunteers. The same measurements were taken for a group of patients with known history of low back pain. Twenty-eight patients with low back pain and sciatica were included for the study. The mean age for this group was 45 years (range 19–74 years), the mean body weight was 68 kg (range 45–88 kg), and the mean body height was 165 cm (range 155–182 cm). The clinical diagnoses were as follows: disc herniation in 16 patients, and spondylosis in 12 patients. MRI scans were done for all cases to clarify the status of the lumbar intervertebral discs with regards to their water content. Having done MRI scans for those patients, disc degeneration was graded in relation to its water content. Depending on the visual brightness of the discs on the T2-weighted sagittal image, the degree of degeneration was graded on a 1 (normal) to 4 (severely degenerated) scale. Total loss of nuclear signals (observed as a completely blackened disc on a T2-weighted image) was graded as Grade 4. Grades 2 (mildly degenerated) and 3 (moderately degenerated) indicated intermediate signal intensities between the two extremes. Independent orthopaedic surgeons with no prior knowledge of the intervertebral disc pressure measurements were asked to make the MRI interpretations.

Sato et al. [1999] measured the intervertebral disc pressure with each individual in one of eight different body positions: prone, standing upright, lateral decubitus, standing

in extension, sitting upright-unsupported, sitting in flexion, and sitting in extension. In all the tested positions, the intervertebral disc pressure was recorded in both the vertical and the horizontal directions. Lateral view radiographs were obtained of all participants while standing and sitting to confirm adequate placement of the needles. The experiments showed that in normal discs the pressure exhibits rhythmic waving in line with respiratory movements while volunteers were in the prone position. This respiratory movement in the disc pressure almost disappeared in the standing and the sitting positions. The cycle of the waving pattern is completely synchronized with the number of respirations. Furthermore, when breathing stopped, this phenomenon disappeared. Valsalva manoeuvre caused consistent transient increase of the disc pressure. In healthy individuals, the average intervertebral disc pressure at the L4-L5 level was observed to be as follows: is 91kPa in the prone, 151 kPa in the lateral decubitus position, 539 kPa in the standing upright position, and 623 kPa in the upright sitting unsupported body positions. The maximum observed intervertebral disc pressure was 1324 kPa in the standing with forward flexion position.

Now, moving to the comparison between normal and degenerative discs, Sato et al. observed the influence of disc degeneration on the intervertebral disc pressure. In this study, the mean intervertebral disc pressures in each grade for the prone body positions was: 91 +/- 25 in Grade 1, 72 +/- 42 in Grade 2 (mild), 32 +/- 45 in Grade 3 (moderate), and 10 +/- 20 in Grade 4 (severe). Based on these observations, Sato et al. concluded that the intervertebral disc pressure is reduced as a result of increasing degeneration grade.

The pressure sensor used by Sato et al. [1999] was manufactured by Tokai Rika (Aichi, Japan). The principle on which this pressure-measuring device operates is based on the piezo-resistive effect of semiconductor strain gauges. It is made of a semiconductor silicone diaphragm using a full-bridge gauge to form a Whetstone bridge with four p-type piezo-resistors. It generates an output voltage proportional to the pressure applied. The sensing diaphragm is mounted on the side of a 178mm long, 1.2-mm-diameter stainless steel spinal needle.

Chapter 3

Animal Spinal Models for Scientific Research Purposes

This chapter discusses the use of animal tissues for scientific research purposes. In more detail, it discusses the developmental, anatomical and biomechanical differences between human and animal spines. Furthermore, it explores the limitations of using the animal models for scientific research purposes. Finally, it discusses the effects of freezing on the biomechanical properties of the intervertebral disc during experiments.

3.1 Animal Tissues for Scientific Research

In different scientific tests, including spine-related experiments, specimens obtained from human donors are considered to be the ideal option. In practice, however, this option is hindered by the difficulties in obtaining the specimens and by the variable degrees of degeneration that are likely to be affecting most of those specimens. As such, the use of animal models for basic experimental research has become the cornerstone for developing medical science in general, and spinal research in particular [Olmarker, 1999]. More specifically, in spinal research, specimens are often obtained from domesticated animals like calf, pig and sheep. These are typically used for both the assessment of a new therapeutic implant as well as studying pathophysiological basics for research in spinal pathology.

"*Animal ethics*" is a common issue that always needs to be considered among scientists when dealing with animal specimens. In this context, given an increasing awareness within the scientific community, it has been agreed that animal rights must not be violated at any stage; they must be always respected and protected [Olmarker, 1999]. Historically, scientists were considered to be able to evaluate the issue of animal ethics; however an increasing demand for more strict regulations is enforced nowadays.

While animal ethics may be considered a limiting factor for scientists conducting animal experiments, it remains a reasonable mandatory pre-request. Also, while no ethical laws must be violated in the laboratories, there have been cases where scientists, in their pursuit of knowledge, have forgotten to preserve the respect and dignity of the animals involved [Olmarker, 1999]. There is a growing sense that the awareness of animal ethics must not simply be a trend that quickly passes by. Instead, the scientific community must constantly accept, respect and implement those ethics. This obviously requires careful planning and evaluation for the relevance of the experiments performed as well as the consideration of any alternative whenever possible. Considering the aforementioned, using in-vivo animal studies were avoided in this dissertation. Animal specimens used for the experiments of this dissertation were obtained from domestically available tissues.

3.2 Differences between Human and Animal Spinal Models for Research Purposes

This subsection discusses the differences between the human and animal spinal models. Here, the developmental, anatomical and biomechanical differences will be discussed separately. After that, the subsection discusses loading differences on the spinal segments and intervertebral discs. Finally, limitations of animal models are discussed.

3.2.1 Differences in the Development of the Spinal Segments

In general, mammalians share a common developmental pathway for the vertebral columns including the IVD. The vertebral column is derived from a mesenchymal tissue aggregation

around the notochord (see Chapter 2 for more details). Comparing the overall development process in human to other mammalian species, some subtle but important differences exist [Alini et al, 2008]. More specifically, differences include the following:

- A human IVD accumulates some notochordal cells within the central portion of the nucleus pulposus. The number of these cells rapidly declines after birth, and by adulthood no notochordal cells will be present in the human nucleus. However, in some other species such as mice, rat, cats, pigs and rabbits, the number of notochord cell population is retained throughout much of the animal's adulthood life. Nevertheless, some other animals, such as cows and sheep, indeed resemble humans as they have some notochordal cells at birth but then the number of those cells declines rapidly as the animal grows. Horses, on the other hand, have no such cells at birth. More interestingly, dogs are considered as two types, the chondro-dystrophoid. The first type, called dachshunds, loses the notochordal cells soon after birth, while dogs of the other type (i.e., the non-chondro-dystrophoid dogs) retain their notochordal cells throughout life. While dogs of the former type are known to often develop disc-related pathologies (e.g., disc prolapses), dogs of the latter type have fewer disc-related pathologies [Alini et al, 2008]. In animals used to study degenerative diseases, the notochord cells population is of important relevance. When compared to the adult human nucleus pulposus, animal notochord cells have a completely different function and morphology. In particular, they are larger and highly vacuolated with many cytoskeletal markers. They also produce large amounts of hyaluronan and have many gap junctions. They often form groups or clumps of cells [Hunter et al, 2003]. Although the exact role of notochord cells remains unknown to date, it has been suggested that those cells are the progenitor as well as the orchestrating cells for the nucleus pulposus development. They directly synthesize the matrix proteins and then differentiate into the mature chondrocytic nucleus cells. They may also help recruiting and coordinating other mesenchymal cells to synthesize the extracellular matrix [Alini et al, 2008].

- The other main variation between human and animal intervertebral disc development is related to ossification centres. In this context, the primary and secondary ossification centres develop in most mammals including human. However, in animals, the

secondary ossifications centres arise at both cranial and caudal aspects of the same vertebral body, forming complete osseous plates. On the other hand, in humans the secondary centres are restricted to the circumferential parts of the vertebrae adjacent to outer annulus, forming what is known as "the epiphyseal ring". These rings fuse by the age of twenty five. They act as the '*growing region*' for the vertebral body until that age. In many other mammals, including sheep and cows, the entire epiphysis and its adjacent physis persist effectively within the vertebral body throughout life, see Figure 3.1 [Alini et al, 2008].

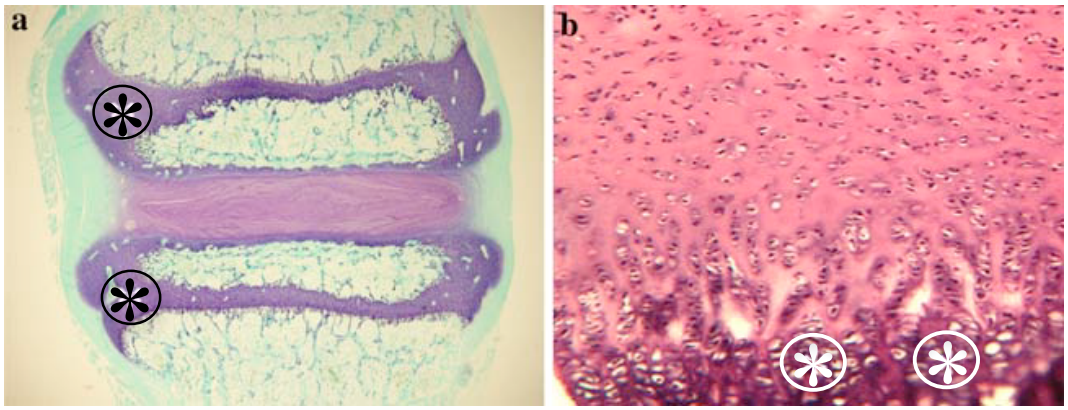

Figure 3.1 The growth plates (asterisks) in the vertebral bodies of a sheep, unlike (b) human restricted to the base of the cartilage endplate (CEP), interfacing between the disc and vertebral body. (Adopted from Alini et al, 2008)

3.2.2 Differences in the Anatomical Variations

The shapes, profiles and relative sizes of the intervertebral discs and its adjacent spinal tissues vary in different animal models. When considering the antero-posterior diameter of the vertebral endplates in humans, it steadily increases in diameter from the cervical to the lumbar region. On the other hand, in large quadrupeds such as calves, sheep and pigs, the antero-posterior diameter remains almost the same. In calves' spines, the lumbar end-plate diameter is close to that of humans [Wilke et al., 1997(A)]. Similarly, when comparing disc heights in animal and human spines, they are constant from the cervical to the lumbar regions in humans. On the other hand, animal cervical discs have large heights while the lumbar discs have small heights [Boszczyk et al, 2001]. The shape of the IVD could also vary from one species to another as follows. Human lumbar discs are convex on both cranial and caudal aspects, while in some animal species (such

as calves and pigs) discs have a convex surface cranially and a concave surface caudally. [Elliott and Sarver, 2004]. Figure 3.2 [Alini et al, 2008] shows discs in different species.

Figure 3.2 Discs in different species. From left to right: human lumbar, L4–L5; bovine tail, C1–C2; sheep thoracic, T11–T12; rat lumbar and tail (arrows show the intervertebral disc location). (Adopted from Alini et al, 2008)

3.2.3 Differences in the Biomechanical Variations

The anatomical variations in the morphology and dimensions are significant. They influence the biomechanical properties of the spinal motion segments in animals. The segmental range of motion in different species has some differences compared to that of human spine. In more detail, the axial rotation of an animal's lumbar spine motion segments is relatively restricted when compared to that of the thoracic and cervical spine motion segments in the same animal. Furthermore, the lumbar spine motion segment in animals is restricted when compared to that of humans [Panjabi, 1990]. These differences are more pronounced in flexion and extension movements. Figure 3.3 [Alini et al, 2008] shows the range of movements in the lumbar motion segment in human, calf, sheep, pig and kangaroo. In humans, most of the flexion/extension movements of the trunk are produced by the lumbar spinal segments. This is not the case in calves, sheep and pigs for example. Such differences must be considered when choosing animal models for studying IVD disorders. They have an indirect role in measuring IVD deformation. They are also some of the major factors affecting degeneration/regeneration processes. One theory for explaining the reduced level of proteoglycan metabolism at the lumbosacral junction

in humans is due to the higher degree of flexibility at this level [Taylor et al, 2000].

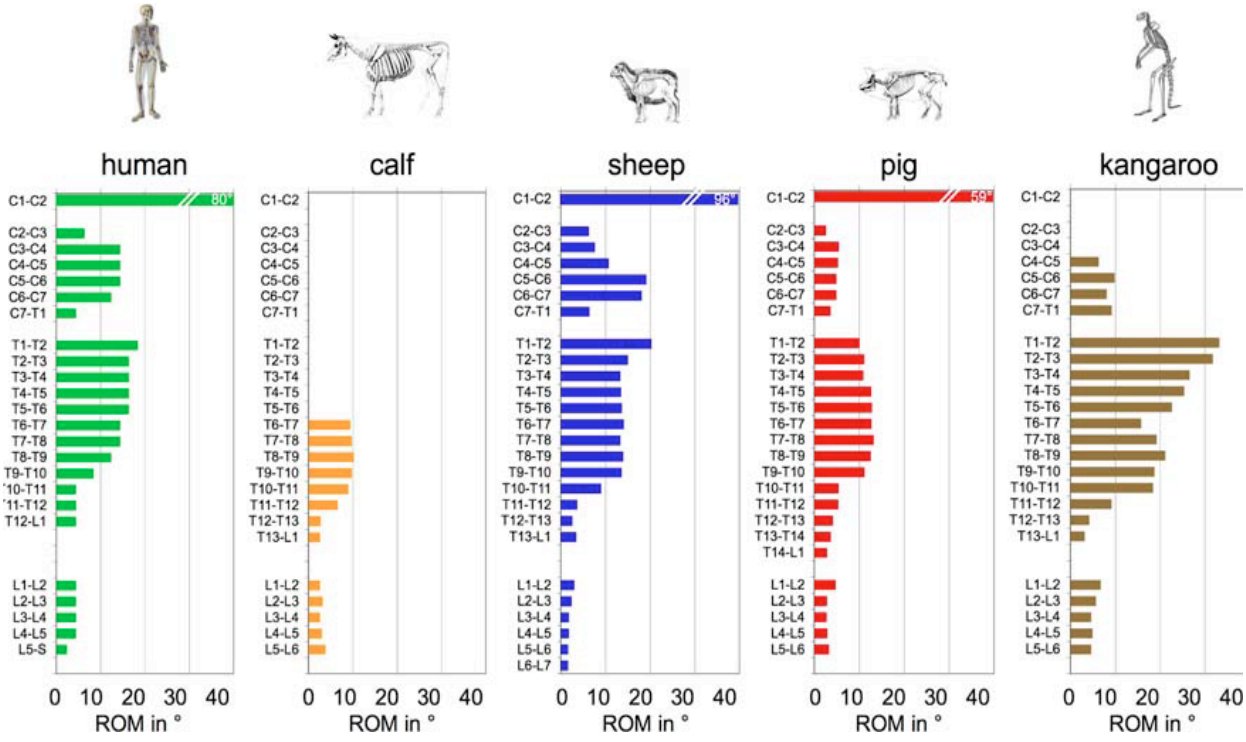

Figure 3.3 The range of movements in the Lumbar motion segment in human, calf, sheep, pig and kangaroo. (Adopted from Taylor et al, 2000)

3.2.4 Loading Differences on the Spinal Segments and Intervertebral Discs

Human lumbar vertebrae are subjected to loading by the upper part of the human body contrary to the case in quadrupeds. As humans acquire an erect posture, it is often assumed that loads on the human spine are greater than loads on the same segment in quadruped spine. Nachemson [1959, 1981, 1999] pioneered the research studies validating this principle. In fact, stabilizing the horizontally aligned spine in animals requires higher passive tension to be generated by the vertebral column muscles and ligaments. In human spine, stabilizing an almost vertically well-balanced and well-aligned vertebral column does not require much force. Although literatures did not compare the direct forces between animal and human spinal motion segments, lumbar spine loading is larger in quadrupeds than in humans [Alini et al, 2008]. This is consistent with the fact that bone mineral density is four folds higher in sheep, calf and pig lumbar vertebral bodies compared to that of humans [Wilke et al., 1999]. While considering small quadrupeds

such as rabbits, mice and rats, smaller forces are needed by muscular and ligamentous tension to stabilize the spine. Therefore, spines of these animals are loaded by less force than human spine. However, they have equal IVD pressure values compared to those in human since the diameters of their discs are much smaller.

Sheep spines are considered as convenient, economical and practical models for spinal research. They are useful for investigating fusion devices, growth factors, disc replacement prosthesis, and instrumentation techniques such as augmenting the vertebral body using cement. Comparative studies showed that the motion characteristics of the intact spines for calves and sheep are similar to those in the human spine. Furthermore, the anatomy of the lumbar spine for these species is qualitatively similar, although the size is considerably different [Kettler et al., 2007].

In their study, Wilke et al. [1997(B)] compared the mechanical properties for both human and sheep spine. They showed that responses to different load directions as well as the range of movement for both groups are similar in cranio-caudal trends. Examples include the following:

- Flexion and extension in the upper thoracic spine is relatively small.
- Lumbar spine axial rotation is relatively small.
- Considering the entire length of vertebral column, both groups have relatively large lateral bending.
- In the mid-cervical spine, the range of motion is large in all three directions. In addition, the C1-C2 segment has a very large range of motion (about 100° in axial rotation).

3.2.5 Limitation of Animal Models

The dimensions of vertebrae in quadruped animals are significantly different compared to humans. Also, bone density in sheep vertebral body is much higher than in humans. Skeletally mature (> 3½ years old) sheep are used in most studies except where growth disturbances such as scoliosis are being studied [Turner, 2005].

3.3 Effects of Freezing on the Biomechanics of the Intervertebral Disc

Storing anatomical specimens for research purposes is only possible if a reliable method for preserving the animal tissues is available. Freezing (at -20°C) is the simplest and least expensive method for storing spinal specimens. Other modes of storage may include the cryo-preservation and lyophilisation. In experimental practice, the aim is to maintain the anatomy and physiology as close as possible to a fresh state. Since bones are the most extensively studied tissue in spinal research, it has become generally agreed that no biomechanical modifications in bones take place after freezing at low temperatures (-20°C or below) [Gleizes et al., 1998].

Although various studies have shown that freezing at -20° C does not damage the elasticity of the tendons and ligaments [Matthews and Ellis, 1968], data for the intervertebral disc are rare [Gleizes et al., 1998]. Studies showed that intervertebral discs undergo morphologic and biomechanical degeneration in fresh air, especially when this air is dry and warm [Galante, 1967]. Storage of these discs by immersion in aqueous normal saline solutions produces impairment changes to its biomechanical properties (decrease in their rigidity after 5 hours of immersion) [Galante,1967]. Flynn and Rudert [1990] compared the biomechanical behaviour of the L2-L3 intervertebral disc in terms of rigidity in flexion/extension and lateral bending following two weeks of freezing at -18° C and after lyophilization. Their study showed significant decrease in rigidity after lyophilisation. Gleizes et al. [1998] showed no significant difference in the rigidity between the fresh and frozen specimens. They also showed that simple freezing at -18°C does not affect the elastic behaviour of the intervertebral disc. In the same experiment, the macroscopic examination did not show any impairment of the spinal segments (i.e., colour or consistency) due to freezing at -18°C. Flynn and Rudert [1990] found the same appearances after two weeks' freezing of fresh discs. This is explained by the fact that tissues with few cells, such as tendons, fasciae and intervertebral discs, are less sensitive to freezing than tissues rich in cells (e.g., nervous systems or muscles) [Gleizes et al., 1998]. Freezing may cause dysfunction of cell metabolism as it causes modification of intra cellular pH and stops the release of proteolytic enzymes. However it also leads to the formation of intracellular and extracellular '*ice*', leading to cytolysis [Meryman, 1960]. Particularly in the case of the intervertebral disc,

this cytolysis, in addition to the presence of catalytic enzymes, leads to a drop in the level of proteoglycans. This, in turn, leads to a drop in the osmotic pressure [Bass et al., 1997]. The amount of osmotic pressure determines the biomechanical behaviour of the discs. When freezing animal specimens, the process of freezing and thawing must be limited as much as possible to avoid damaging the tissues [Matthews and Ellis, 1968]. It should also be noted that the thawing process should be in a moist environment. Gleizes et al. [1998] showed that the biomechanical behaviour of the intervertebral discs, in terms of flexion/extension rigidity and right/left lateral bending, remains similar whether the vertebral column is fresh or has been frozen for up to 3 months. Simple freezing at a temperature of -18°C is a convenient, easy and reliable method of storage. This method of storage allows laboratories of biomechanical research to regularly obtain anatomic specimens of good quality that can be biomechanically tested without introducing experimental bias.

Several investigators accepted freezing the animal models for research purpose. In particular, the literature supports the following [Turner, 2005]:

1. The elastic characteristics of different tissues including bones, ligaments and tendons are not significantly altered by storage at up to -20°C.
2. When considering the IVDs, the process of freezing does not alter the elastic tensile stiffness of the annulus fibrosus.
3. *X*-rays diffraction demonstrated that freezing does not alter the arrangement of annular collagen fibrils.
4. Freezing has no effect on the hydrostatic pressure of the nucleus. The elastic stiffness of intact IVD in compression is similarly maintained.

Chapter 4

Description and Validation of the Methodology

This chapter starts by describing the basic principles of pressure and its measurements (Section 4.1). Then, the proposed pressure sensor layout is presented and validated (Section 4.2). The final experiment setup is then proposed, and the obtained results are analysed (Section 4.3).

4.1 Principles of Pressure and Pressure Measurements

This section is divided into three subsections. The first describes the basic principles of pressure, while the second describes how to measure pressure in general. Finally, the third subsection describes the piezoelectric effect—an important pressure sensing effect that will be used later on in Section 4.2.

4.1.1 Basic Principles of Pressure

Generally speaking, pressure P is defined as a force F exerted on a surface area A. That is,

$$P = F / A$$

Since liquid behaves as a continuous medium, any pressure imposed on a liquid at rest is transmitted undiminished to all parts of the liquid and to the walls of the container [Wilson, 2002]. A container filled with liquid contains innumerable atoms and molecules that are constantly bouncing off its walls. The pressure would be the average force that is imposed by these atoms and molecules on a single unit of area of the container. Pressure does not necessarily have to be measured along the entire wall of the container; it suffices to measure it on a single

unit of area anywhere on that wall. In clinical terms, *blood pressure,* for example, is generated by the atoms and molecules of blood pushing against the surface area of blood vessels. Similarly, the *alveolar pressure* is generated by the air molecules that are pushing against the alveoli.

According to Pascal's law—an import law in physical sciences—applying a force F_1 on a certain surface area A_1 results in pressure, $P_1 = F_1/A_1$, that is transmitted throughout the liquid within the container. Next, this law is explained in more detail as it is considered to be the corner stone for understanding the principles of pressure and its measurements. To this end, the hydraulic jack will be used as an example since the way it works depends entirely on Pascal's law. An illustration of the hydraulic jack is provided in Figure 4.1. In more detail, when applying a force F_1 to the piston with surface area A_1, the resulting pressure, $P=F_1/A_1$, will be transmitted throughout the liquid within the jack to the other end of the jack (see Figure 4.1). Since the pressure stress is equal throughout the volume of the liquid, the liquid exerts equal pressure on all parts of its container. So, P is exerted equally on all points of the structure of the hydraulic jack liquid system. At the piston with surface area A_2, since the pressure remains unchanged, the generated force, denoted as F_2, is computed as follows:

$$P = F_1/A_1 = F_2/A_2$$

Therefore,

$$F_2 = (F_1/A_1) \times A_2$$

This means that a small force F_1 applied on surface area A_1 of the piston results in a large force F_2 being generated on surface area A_2 of the piston. It should also be noted that the volume of liquid moved by A_1 is the same as the volume displaced by A_2, and since the surface area A_2 is greater, the same volume results in a shorter displacement [Wilson, 2002].

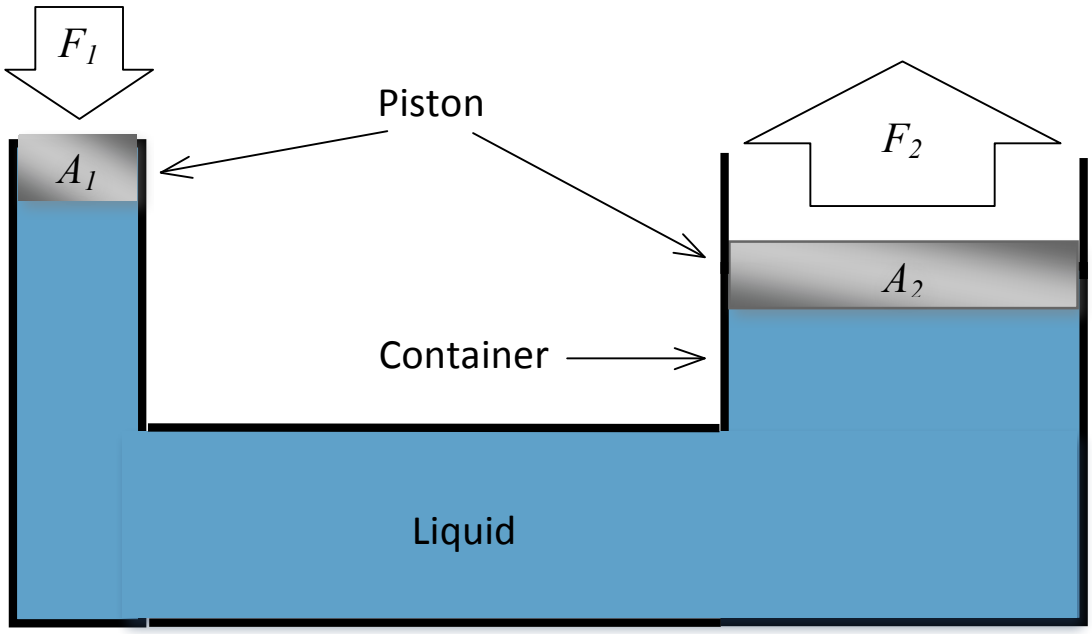

Figure 4.1 Illustration of Pascal's law in hydraulic jacks

Using the same principle, it is possible to measure the arterial blood pressure using a fluid-filled, air-free, tubing system connected to a pressure sensor device. Note that, in a real hydraulic jack, a reservoir of liquid and a valve-checking system are included in the same system, and this allows for repeating the stroke of piston A_1 without losing the displacement of A_2.

4.1.2 Principles of Pressure Measurement

There are different units for measuring pressure. One such unit is *SI*, also known as the *Pascal* (*Pa*), which is equal to one *Newton* per square meter. That is, $SI = Pa = N/m^2$ [Giancoli, 2004]. Other commonly used units of measurements include: *pounds per square inch (psi), atmospheres (atm), inches of mercury (inHg or "Hg)*, and *millimetres of mercury (mmHg)*. Throughout this dissertation, only the *psi* unit of measurement will be used.

Pressure measurement can be classified into *static* or *dynamic* [Wilson, 2002]. Specifically, the pressure in cases where no motion is occurring is referred to as *static* pressure. Examples include

the pressure of the air when the alveoli of the lung are filled of it, or the pressure of the blood when the ventricles of the heart are filled of it. The motion of a liquid, on the other hand, changes the force applied to its surroundings. Such a pressure measurement is described as *dynamic*. Examples include the pressure inside the alveoli while air is being let out of the lung, or the pressure inside the ventricle while blood is being pumped out of the heart.

Pressure measurement can also be classified based on the type of measurement being performed. In particular, there are three main types of pressure measurements: *absolute*, *gauge*, and *differential*. In more detail:[1]

- *Absolute pressure* measurement is considered relative to vacuum as shown in Figure 4.2 below. The abbreviations PAA (Pascal's Absolute) or PSIA (Pounds per Square Inch Absolute) are often used to describe absolute pressure. For example, reading the oxygen tension in the arterial blood gas sample is an absolute pressure reading.

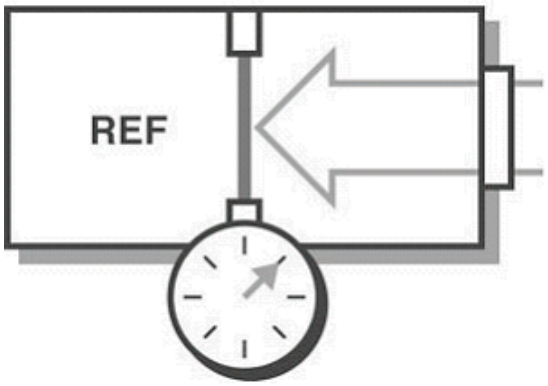

Figure 4.2 Absolute pressure sensor

- *Gauge pressure* is measured relative to ambient atmospheric pressure as shown in Figure 4.3. The abbreviations PAG (Pascal's Gauge) or PSIA (Pounds per Square Inch Gauge) are use to describe gauge pressure. For example, intra-alveolar pressure is a gauge pressure being measured relative to ambient atmospheric pressure.

[1] The figures used to describe the differ types of pressure measurement (namely, 4.2, 4.3, 4.4 and 4.5) were all obtained from the *national instruments* webpage: http:// www.ni.com/white-paper/3639/en.

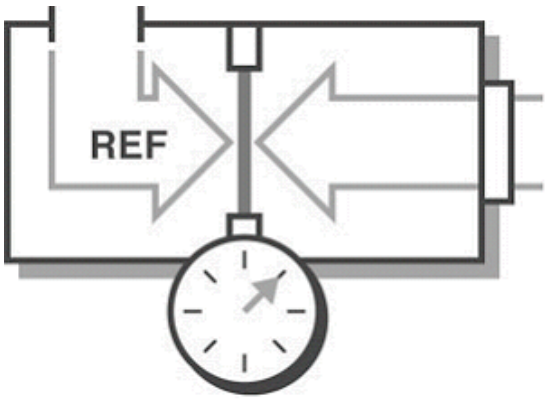

Figure 4.3. Gauge pressure sensor

- *Differential pressure* is similar to gauge pressure, but instead of measurements being relative to ambient atmospheric pressure, they are taken with respect to a specific reference pressure as shown in Figure 4.4. The abbreviations PAD (Pascal's Differential) or PSID (Pounds per Square Inch Differential) are used to refer to differential pressure (e.g., describing blood pressure as "millimetre of mercury" is a differential pressure; it is taken in reference to the column height of mercury).

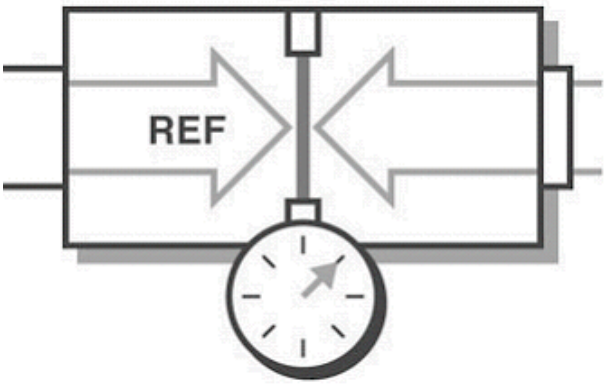

Figure 4.4. Differential pressure sensor

Having described the basic principles of pressure and its measurement, the following subsection describes the "*Piezoelectrical effect"*, which is an important pressure sensing effect that will be used later on during the experiments in Section 4.2.

4.1.3 Piezoelectric Effect for Pressure Sensing

The Piezoelectric effect was first discovered by the Curie brothers (Pierre and Jacques Curie) in the late 19th century. It describes the ability of certain materials to transform mechanical input energy to electrical output. More specifically, when a pressure is applied to a piezoelectric material, it causes a mechanical deformation and a displacement of its electrical charges. Those charges are highly proportional to the applied pressure [Tichy et al., 2010]. Many creatures naturally use piezoelectricity in various interesting ways. Bones, for example, once loaded produce charges proportional to the resulting internal torsion or displacement. Those charges stimulate and drive the build-up of new bone material. This leads to the strengthening of structures. With time, this allows weaker structures to increase their strength and stability as material is laid down proportional to the forces affecting the bone. Piezoelectric pressure sensors (Figure 4.5) use stacks of piezoelectric crystal or ceramic elements to convert the motion of the force-summing device to an electrical output. Specially formulated ceramics can be artificially polarized to be piezoelectric, and they have higher sensitivities than natural crystals [Wilson, 2003]. The wide spread of piezoelectric sensors is directly related to a set of inherent advantages, such as the fact that they are insensitive to electromagnetic fields and radiation, enabling measurements under harsh conditions. Moreover, although these sensors are electro-mechanical (i.e., systems that react to compression), the sensing elements show almost zero deflection.

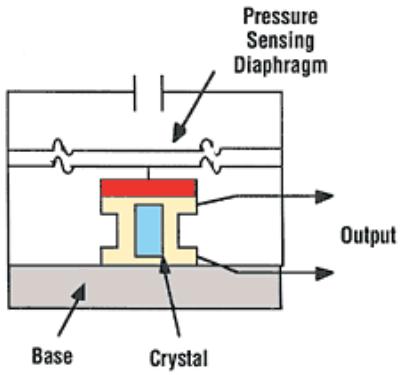

Figure 4.5. Piezoelectric pressure sensors use stacks of piezoelectric crystal or ceramic elements to convert the motion of a force-summing device to an electrical output.

4.2 Pressure Sensor Layout and its Validation

This section first describes the proposed pressure sensor layout (Section 4.2.1). It then presents two alternative methods for validating this layout: the first method (in Section 4.2.2) uses a *calibrator*, while the second one (in Section 4.2.3) does not.

4.2.1 Pressure Sensor Layout

As a base for the pressure sensor layout, the following gauge-sensor was used: "Honeywell Miniature Signal Conditioned 40PC series[2]" with a pressure range of 0-15 *psi* (see Figure 4.6). The reason behind choosing this particular gauge-sensor is that it has several desirable features, including: conveniently small size, amplified sensing, suitability for operation under temperatures ranging from -45^{O} to +125^{O}, use of piezoelectric technology, and accuracy of 0.2%. However, its drawback is that it provides pressure recordings that are not represented in standard pressure units such as psi, for example. To convert the recordings into such a unit of choice, one needs to multiply the recordings by a numerical constant. This constant needs to be computed each time the sensor is switched on (see Section 4.2.2 for more details).

Figure 4.6 40PC-series pressure sensor.

[2] See http://sensing.honeywell.com

The sensor was connected to an "Analog input/Digital output" convertor (A/D Convertor -NI USB 6009 -8, 14-bit, 8 inputs, multi-function I/O), which is shown in Figure 4.7. This A/D convertor is used to convert the sensor output from analog to digital format, so that it can be recorded and analysed via a computer.[3] The digital output of the convertor is, in turn, connected to a Toshiba® laptop (Satellite L100) on which a special software is installed to record the sensor output. This software was developed by the author using "LabView 7.1", which is a graphical *programming environment* that provides intuitive graphical items and wires that resemble a flowchart.[4]

Figure 4.7 Signal convertor (NI USB 6009).

The pressure sensor layout, with all the necessary components and connections, is shown in Figure 4.8. As can be seen, a tube is connected from one end to the pressure sensor, and from the other end to a to a needle (BD Microlance™ 3, 19G, 1½" Ref 301500) via a three-way valve. Both the tube and the needle are filled with distilled water using the three-way valve, allowing any air to be expelled out of the system. The pressure sensor was then connected to the signal convertor, which is in turn connected to the laptop on which the software was installed via a USB port.

[3] An electrical power supply unit 9 [v], which is provided separately, is required to operate the A/D convertor.

[4] For more details, see http://www.ni.com/labview.

Having explained the pressure sensor layout, the remainder of this section focus on validating this layout using two different methods: one with a calibrator while the other one is without it.

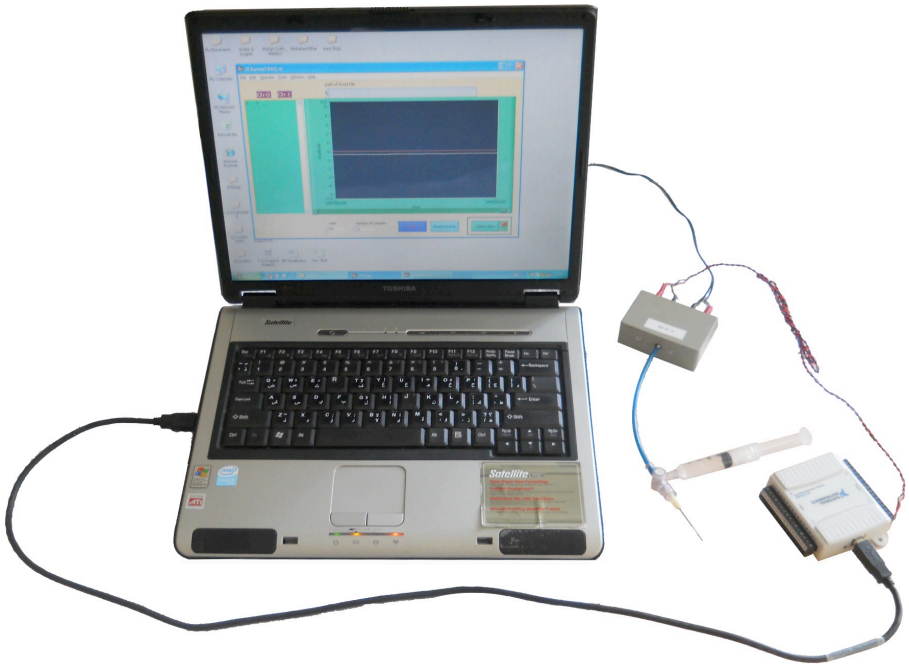

Figure 4.8 The pressure senor layout

4.2.2 Validating the Pressure Sensor Layout using a Calibrator

In this subsection, the basic idea behind validating the pressure sensor layout is to compare the pressure readings (that are obtained from the layout) with the pressure readings that are obtained from a standard calibrator. This comparison is done using a *pressure chamber*, which is connected to both the pressure-sensor device and the standard calibrator. This pressure chamber consists of the following components (see Figure 4.9):

- **A Cylindrical Chamber**, 12*cm* long x 3.5*cm* diameter, with a dial pressure gauge securely attached to its wall. This gauge can be used to detect any possible leakage within the chamber cavity.
- **The Proximal End** of the chamber is made of a metal cap fitted with a polyethylene valve allowing flow in both directions. The inner end of the valve securely holds a 21 *G*

needle (0.8 x 40 *mm* Microlance3®) within the chamber space. The outer end, on the other hand, simply connects the needle to a tube.

- **The Distal End** of the chamber is also made of a metal cap in which a dual way flow valve is fitted.

When connecting the three components of the chamber, it is crucial that all leaking points are sealed firmly since any leakage would affect the consistency of the pressure sensor recording. With this in mind, all potentially leaking points were thoroughly tested and treated. In particular, the distal end was first occluded using polyethylene plug. After that, using a 50 *ml* syringe, air was injected from the proximal end into the chamber, building the pressure up to 25 *psi* as recorded by the attached pressure gauge dial, and allowing the chamber to settle. The chamber was emerged in a basin of water to identify, and treat, any leaking points. This process of injecting air, identifying, and treating leaking points was repeated until no further drop in pressure was observed.

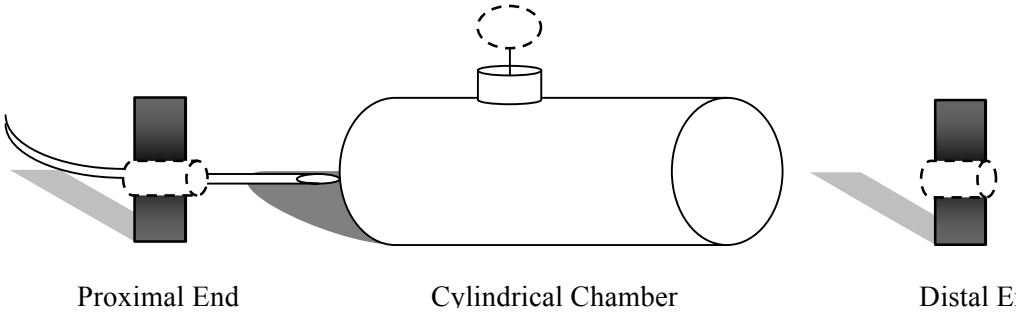

Figure 4.9 Pressure chamber

Having explained how the pressure chamber is structured, it is now explained how the chamber is used to validate the pressure sensor layout. Basically, the chamber is connected to a standard calibrator, as well as the pressure sensor. The pressure within the chamber is then increased, and the reading of both the calibrator and the sensor is analysed. The remainder of this subsection explains the aforementioned procedure in more detail.

From the distal end, the pressure chamber is connected to both, a 50 *ml* syringe, and a standard calibrator, using a T-piece connection, which is shown in Figure 4.10. More specifically:

- The syringe is used to inject air into the chamber so as to build the pressure up. The connection between the syringe and the T-piece is done via a plastic tube pre-fitted with a clip valve, which is closed right after the pressure is built. This is necessary to ensure that the pressure within the chamber will not escape through the syringe during the experiments.

- As for the calibrator, the following model is used: "VT Plus HF Gas Flow Analyser". This calibrator is particularly accurate, user friendly, and, more importantly, has a *zero mode* by which all the sensors within the calibrator are periodically zeroed (i.e., calibrated to a zero reference). This is crucial to ensure that the reading is consistently accurate.[5]

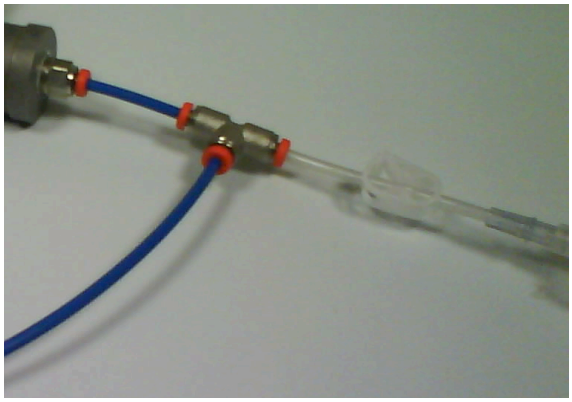

Figure 4.10 T-piece connecting: (i) the distal end of the chamber, (ii) a 50 *ml* syringe, and (iii) a standard calibrator.

[5] Any other reliable, accurate, and user-friendly calibrator with a zero mode can be used.

As for the proximal end of the chamber, it is connected to the pressure sensor using the needle that was fitted in the Proximal End as described earlier in this section. This simulates the needle, which is inserted into the intervertebral disc space in the experiment layout that was proposed in Section 4.2.1. The entire validation setup is shown in Figure 4.11.

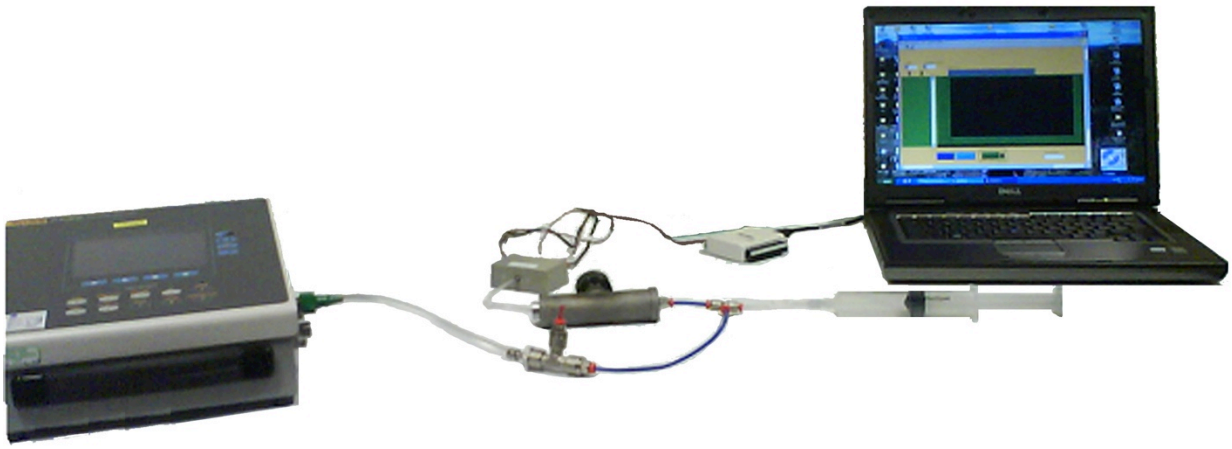

Figure 4.11 The setup for validating the pressure sensor setup using the pressure chamber and a standard calibrator

Experiments were carried out to validate the *Linearity,* i.e., the ability of the sensor to provide readings that vary in a manner directly proportional to changes in the pressure. This is particularly important as it means that the sensor reading can be converted into *psi* values by simply multiplying it by a constant factor. In order to validate the linearity, the pressure sensor recordings were plotted against those obtained (in *psi*) by the calibrator (see Figure 4.12). As can be seen, the recordings grow linearly with the pressure readings. More formally, the R^2 value for the plotted graph was 0.999.[6]

[6] R^2, also kwon as the *Coefficient of Determination*, is a standard measure of "goodness-of-fit" of the *linear regression* in a certain graph. Basically, the value R^2 is a fraction between 0.0 and 1.0. Any R^2 value of 0.0 means there is no linear relationship between the X axis and Y *axis* (i.e., knowing X does not help in predicting Y). On the other extreme, having R^2 equal 1.0 means that all points for a straight line with no scatter, i.e., knowing X enables predicting Y perfectly. For more details see [Draper and Smith, 1998].

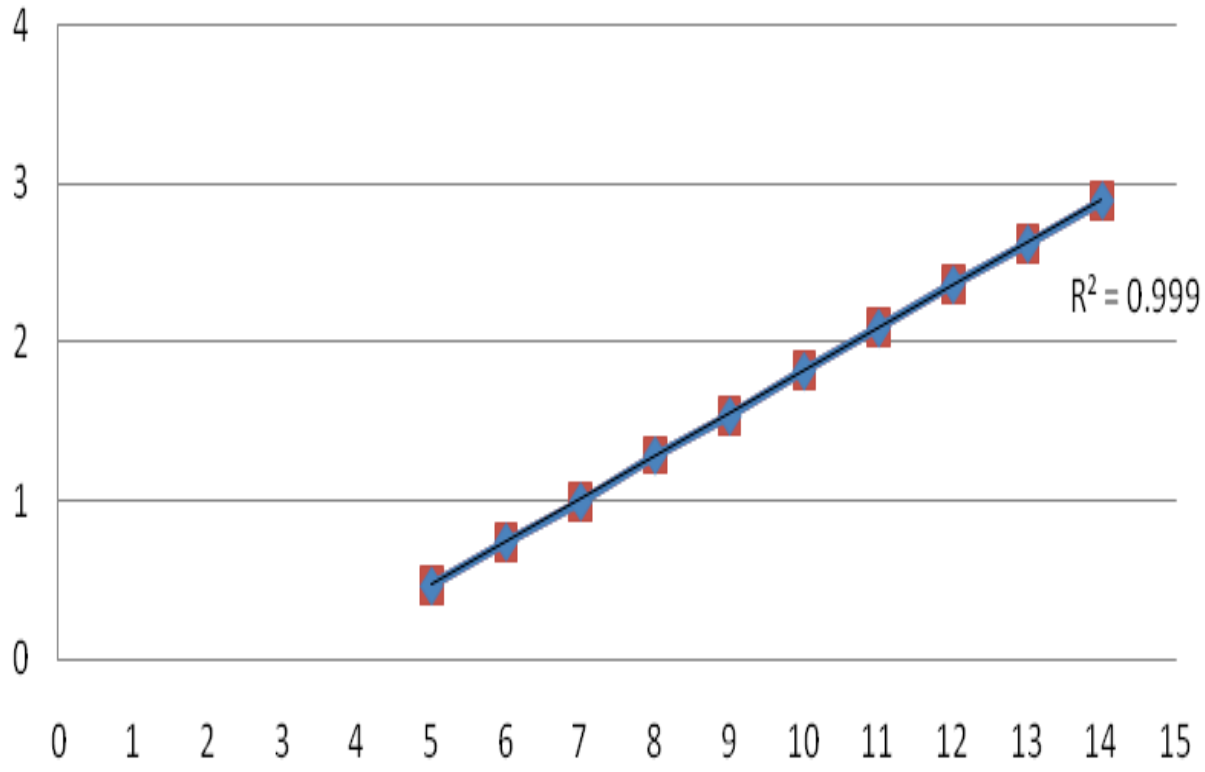

Figure 4.12 Pressure values (*psi*) against the sensor recordings

To confirm the linearity property even further, the experiment was repeated under the same circumstances (after switching the sensor off and then on again). The results of the second experiment were compared with those of the first one (see Figure 4.13). As can be seen, both plots are almost identical, apart from the *bias* in each plot.[7] The linearity of the plot confirms that the bias is a constant that is added to the actual reading. Furthermore, it confirms that this constant remains unchanged throughout a single experiment. This constant is computed as the sensor reading when pressure is equal to zero. In particular, the bias in the first experiment was equal to (- 0.875) and the bias in the second was (+0.516).

[7] Generally speaking, bias in statistics is a systematic favouritism that is present in the data collection process, resulting in misleading results.

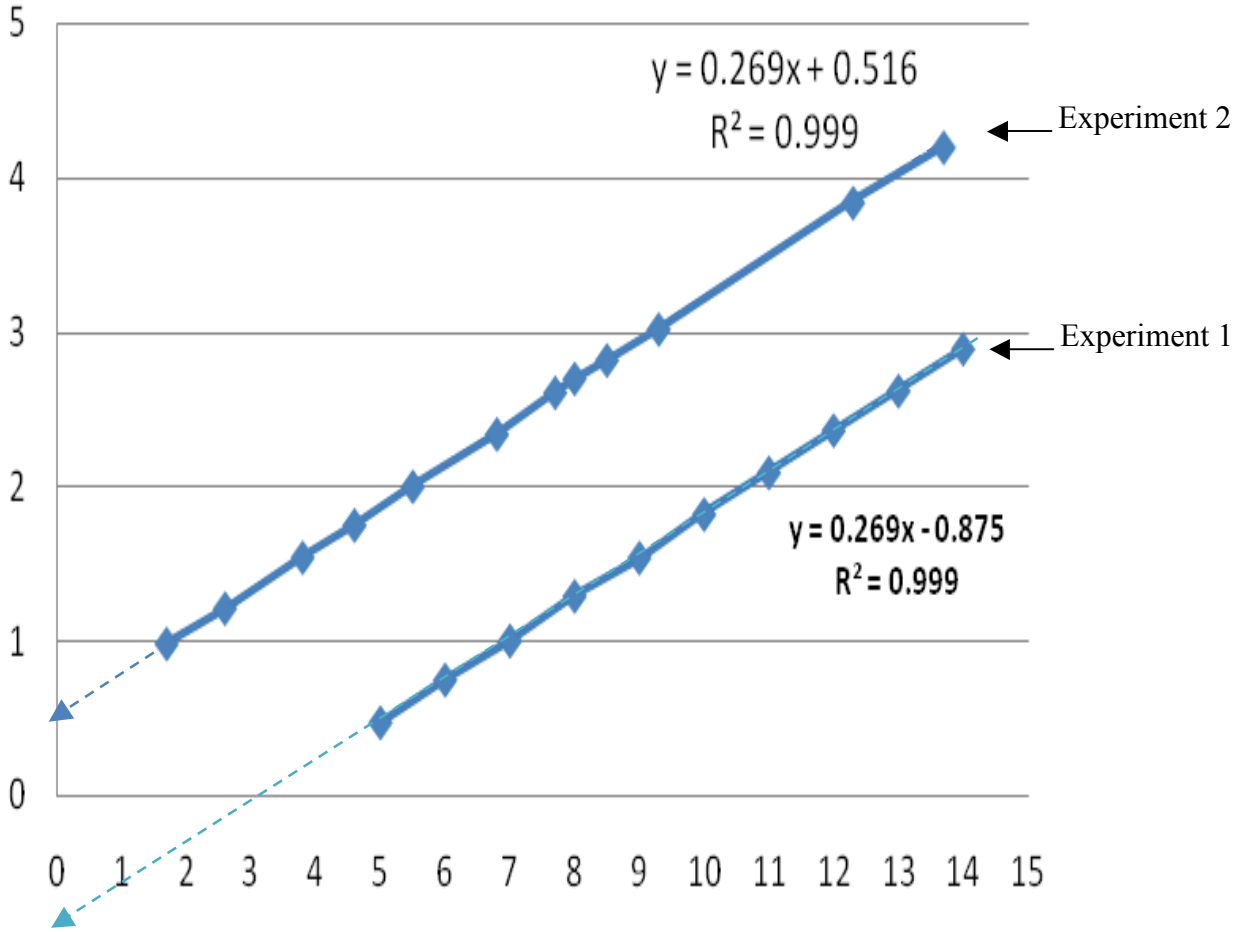

Figure 4.13 Comparing both experiments of linearity. Pressure values are plotted against the sensor recordings.

As discussed above, the bias will affect all obtained results, and so there will be a need for a calibrator to calculate the bias value after every experiment. To avoid this potential problem, the author added a zeroing mode to the software used in the experiments. An example is shown in Figure 4.14, where the results of both experiments are plotted after correcting the bias (using the zeroing mode). As can be seen, by using this correction process, different experiments provide equal results.

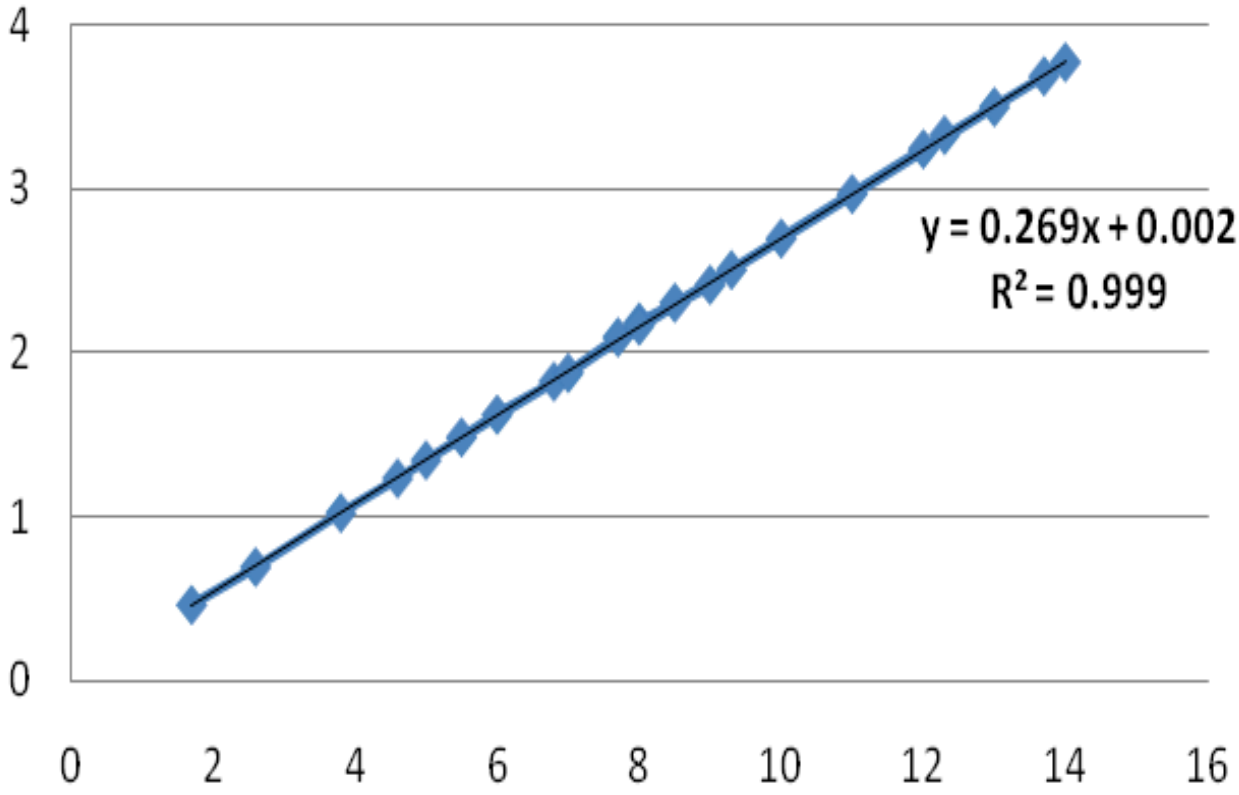

Figure 4.14 The results obtained by Experiment 1 and Experiment 2 after eliminating the bias.

4.2.3 Validating the Pressure Sensor Layout without a Calibrator

In this subsection, an alternative method (which does not use a calibrator) is presented for validate the linearity of the pressure-sensor setup. Unlike the first method that was proposed earlier in Section 4.2.2), this method can be used whenever a calibrator is not available. The basic idea is to apply different amounts of force on a known surface area, and then verify that the sensor readings are proportional to the force, i.e., the ratio between the force and the reading is constant. More specifically, the force is generated by the weight of metallic blocks, which are placed on the vertically-positioned syringe, and the surface (on which this force is applied) is the syringe piston. In order to hold the syringe securely in a vertical position, the syringe was placed in a specially-designed tube, which is called a *holding cylinder*. This cylinder is 120*mm* long, 4*cm* in diameter, and has a rectangular base that allows it to remain vertically stable. To enable a tube to run between the syringe nozzle and the pressure sensor, the holding cylinder was placed

on a metallic frame that was specially designed as follows. The frame dimensions were 130 *mm* long x 120 *mm* wide x 110 *mm* deep. The central part of the frame is hollow, and the frame itself is cut to allow the tube to run through. The holding cylinder and the metallic frame are illustrated in Figure 4.15.

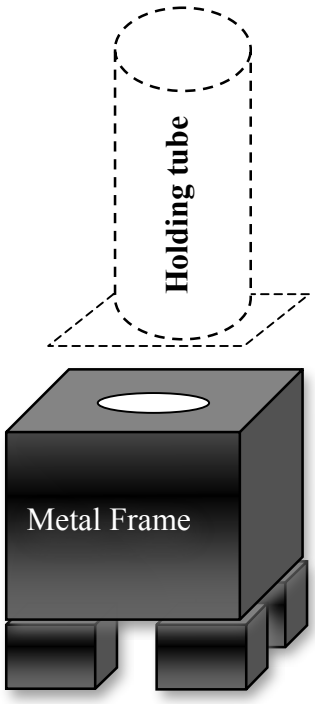

Figure 4.15 The metal frame and holding tube to vertically suspend the syringe and weight blocks.

The experiment was performed with three different-size syringes. The surface area of the piston was calculated for each of the three syringes using the following equation:

$$\text{Circle surface area} = \pi \times r^2 = 3.14159 \times r^2$$

Using this equation, the surface of each syringe was computed based on its radius as follows:

Syringe 1: piston radius (r) = 13*mm* ➔ surface area= 0.00052 m^2.

Syringe 2: piston radius (r) = 10*mm* ➔ surface area= 0.000314 m^2.

Syringe3: piston radius (r) = 8*mm* ➔ surface area= 0.0002 m^2

Three metallic blocks were used, each weighing 260 *g*. The force generated by these blocks was calculated in Newton (*N*) by multiplying the weights in *kg* by the *Gravitational Acceleration factor,* known to be 9.81 (see Figure 4.16). That is:

Force applied by one block = 0.26X 9.81 = 2.55 *N*

Force applied by two blocks = 0.52X 9.81 =5.10 *N*

Force applied by three blocks = 0.78 X9.81 =7.65 *N*

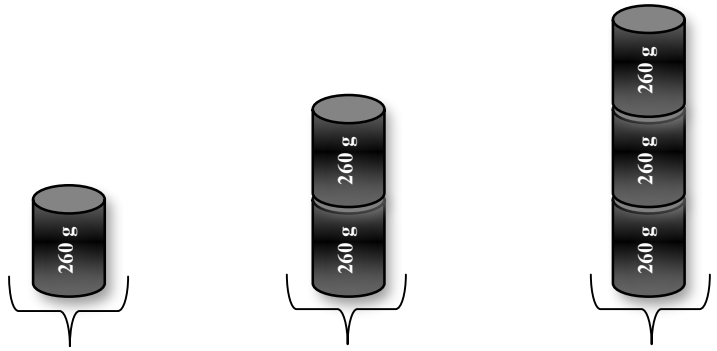

Figure 4.16 The force generated by different combinations of metallic blocks.

Having calculated both the force (*F*) and the surface area (*A*), it is now possible to calculate the resulting pressure (*P*) as follows:

$$P = F / A$$

When calculating the pressure, it should be noted that air, like any other gas, is compressible. This means that, when placing the weights on an air-filled syringe, the pressure recording will not reflect the force being applied. To tackle this problem, the syringes, as well as the tube

connecting, were all filled with water and ensured to be air-free. Figure 4.17 illustrates the entire setup, including all the components and connections.

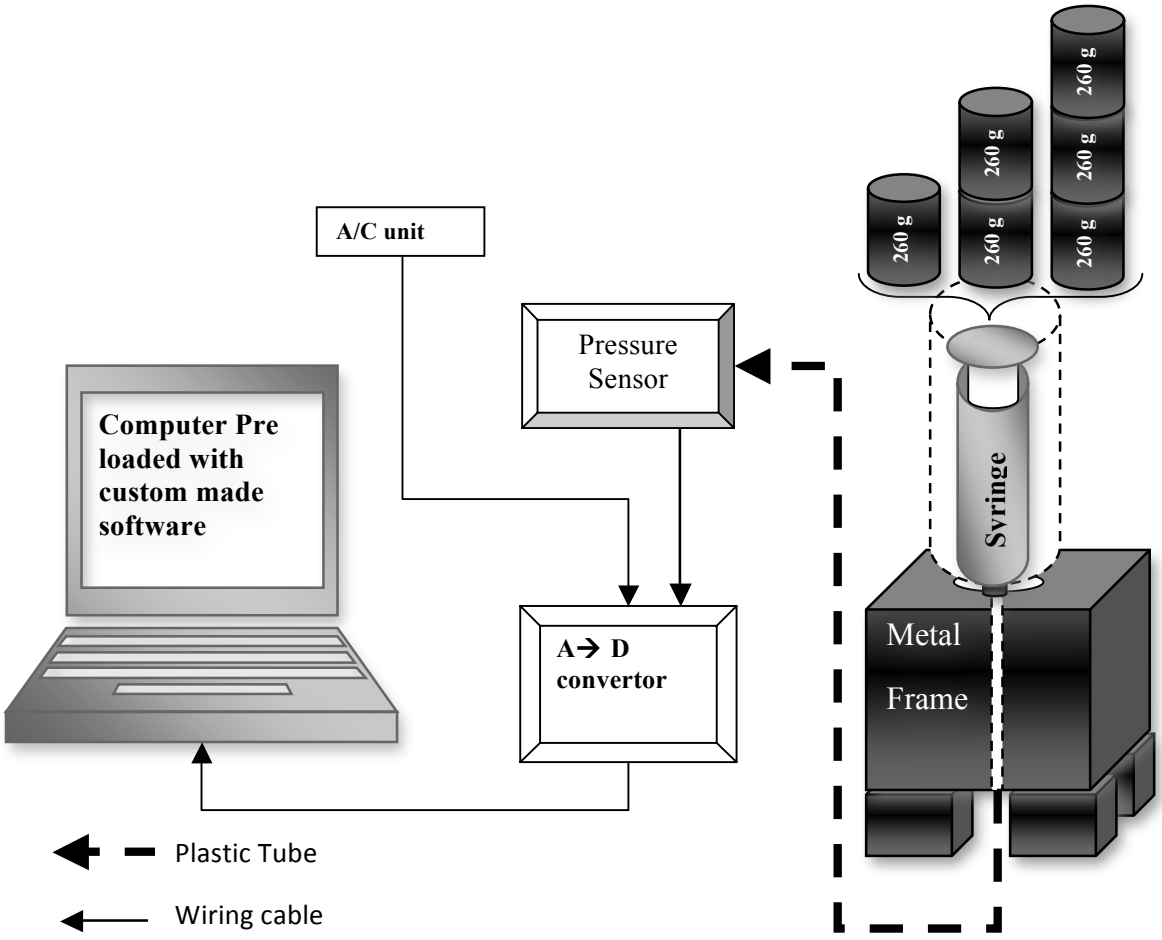

Figure 4.17 The setup for validating the pressure sensor setup without using a calibrator.

The results of the validation experiment are shown in Figure 4.18. In particular, one metallic block was placed on the syringe (weight 260*g*), then two blocks (making the total weight 520*g*), and finally three blocks (weight 780*g*). As can be seen, the pressure sensor recording is proportional to the applied pressure.

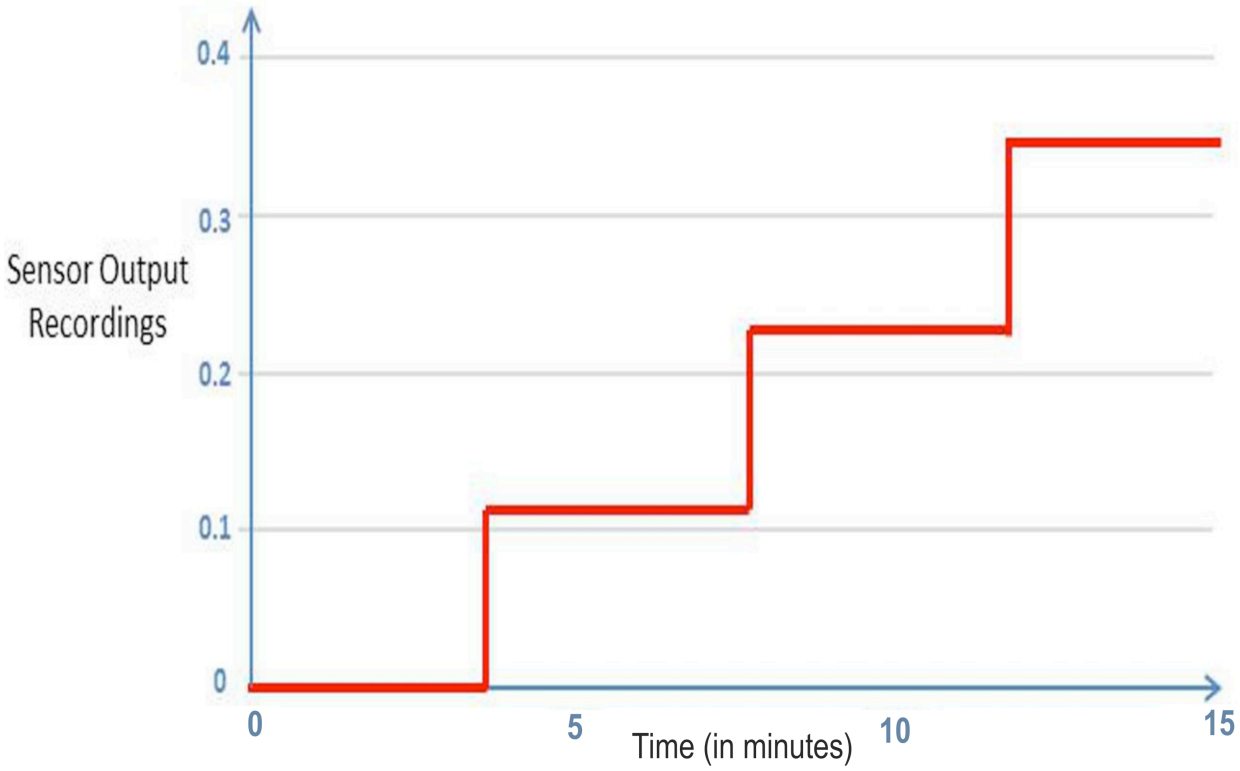

Figure 4.18 Experiment results for validating the pressure-sensor recordings without using a calibrator.

Now that the pressure sensor layout has been described and validated, the following section describes the final experiment setup and analyses the obtained data.

4.3 Methodology

The main goal of the study it to address the following research question:

> *Given any spinal motion segment, will the change in the intervertebral disc pressure follow a constant trend across different specimens when identical deformation is applied under similar conditions?*

The study serves as a "proof of concept". More sophisticated and thorough experiments will be needed to analyse the link between the MR generated images and the obtained pressure readings.

4.4 Pressure Sensor Experiments

In this section, the main goal is to verify whether a deformation of the spinal motion segment leads to a measurable, predictable, change in the intervertebral disc pressure. Specifically, the experiment is designed to demonstrate that:

1. By inserting a pressure-sensor needle into an intervertebral disc, the sensor detects a positive pressure reading.

2. By applying a deformation to the spinal motion segment, the pressure within the nucleus pulposus increases.

3. Increasing the applied deformation leads to a predictable alteration in the pressure reading.

The experiment involves dealing with animal tissues. As such, it is important to use a safe environment that can accommodate animal tissues in order to minimize any potential risks. To do this, the author used the *"tissue lab"* of the Clinical Neurosciences department at the University of Southampton, which is suitable for the purpose of the experiment.

Since the experiment needed to be carried out in the tissue lab, there were certain regulations of this lab that needed to be complied with. In particular, as a preliminary step, the completion of a *risk-assessment form* was mandatory. This form specifies any potential harm associated with each task of the experiment, and outlines the necessary precautions that need to be taken in order to minimize such risks. More details on this form can be found in Appendix A.

Fresh animal specimens are chosen from sheep lumbar spine. Segments from L1 to L6 are obtained within 24 hours from animal slaughter, and are prepared for the experiment as follow: the segments are dissected from the rest of the body. The L5/6 spinal motions segment is used for the experiments. A small window is made on the anterior aspect of the intervertebral disc; a cut in the muscle tissue is done to allow access to the anterior surface of the disc. Care is taken to ensure that no damage is caused to the external surface of the annulus fibrosus while making the cut. For storage purposes, the prepared specimens are frozen at a temperature of $-22C^0$ (for more details on storing animal tissues for research purposes, see Section 3.3). The specimens are placed in clearly-labelled, hard containers to avoid adjacent tissue contamination and avoid any changes in the physical properties of the specimens by being subjected to loads during the storage process. Before starting any experiments, the frozen specimens must be allowed to thaw at room temperature (18 to 22^0C) for 9-12 hours.

In the experiments, a "C-clamp" tool is used to squeeze the spinal motion segment in the vertical axis, resulting in the desired deformation. In more detail, the clamp was rigidly fixed in the vertical position as shown in Figures 4.19 (F). This way, deformation can easily be applied by squeezing the spinal motion segment using the clamp as shown in Figure 4.19 (G and H). In order to quantify the applied deformation, a sensitive scale was placed underneath the specimen and between the two jaws of the C-clamp (see Figure 4.19 (I)). To allow for the scale and specimen to be easily placed in a stable position, a cut was made in a wooden, horizontally-placed board, to accommodate the fixed jaw of the C-clamp (see Figure 4.19 (F)). The specimen was placed vertically on the scale, allowing the C-clamp to apply vertical force by screwing its movable jaw. Next, we explain how pressure is measured while applying different deformations.

The intervertebral disc pressure was measured using the "pressure sensor layout" described earlier in section 4.2.1. In particular, the needle was inserted through the small cut made in the muscle tissue while the specimen was being prepared. Here, it is essential that the needle remains in a fixed position (in relation to the intervertebral disc) throughout the same experiment.

Otherwise, an increase in the disc pressure may cause the needle to be expelled out of the intervertebral disc space. In order to maintain the fixed position of the needle, a special "*needle holder tray*" was designed as follows: an L-shaped bracket (with three holes in each limb) was attached to a wooden base. One limb of the bracket was firmly screwed to the wooden base using three screws, one in each hole of the limb. The three holes in the other (now vertical) limb of the bracket allow for choosing one of three different levels for the needle to be inserted, depending on the size of the specimen in any given experiment (see Figure 4.19 (A)). The entire experiment setup can be seen in Figure 4.18 (I).

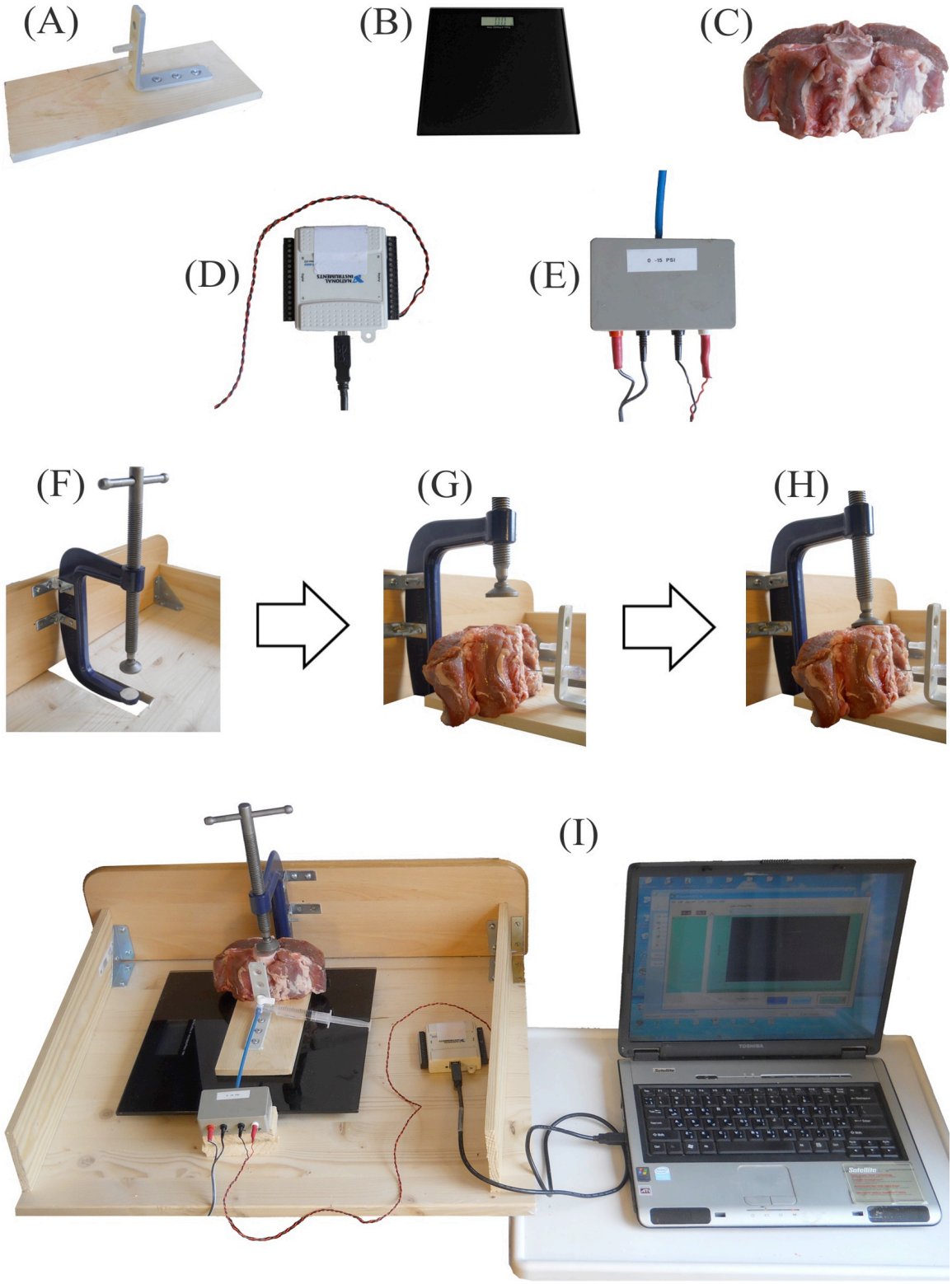

Figure 4.19 The experiment setup. (A): needle-holding tray. (B): scale. (C): specimen. (D): convertor. (E): sensor. (F): C-clamp fixed vertically. (G): specimen in neutral position. (H): specimen under deformation. (I): entire setup.

Having described the experiment setup, it is now explained how the experiment itself is conducted; a step-by-step guide is provided below:

- The specimen is placed vertically on the surface of the needle-holding tray, which in turn is placed on the surface of the scale.

- The needle of the "pressure sensor layout" is passed through the most suitable hole (out of the three holes in the vertical limb of the bracket on the needle-holding tray), such that it matches the disc level in the vertical plane. While being inserted into the intervertebral disc, the needle is filled with distilled water. Here, it is essential to detect any air bubbles carefully, and evacuate them prior to starting the experiment as any such bubbles can significantly compromise the results obtained.

- The pressure sensor is placed at the same level of the selected intervertebral disc. From one end, the pressure sensor is connected to the signal convertor as described in Section 4.2.1. From the other end, the pressure sensor is connected to the needle via a polyethylene tubing system. The tubing system is filled with distilled water, and air bubbles are evacuated from the tubing system.

- The sensor is switched on and the software is started while the tube remains unconnected to the needle. The reading obtained at this stage is considered as zero pressure reading. While the software is running, the tubing system is fastened to the needle inserted in the intervertebral disc.

- Readings are collected over one to two minutes prior to applying any deformation to the intervertebral discs. Readings collected at this stage represent the intervertebral disc pressure in neutral (resting) position.

- The specimen is squeezed between the jaws of the C-Clamp until the scale reads 10kg. To prepare for this step, the needle-holding tray is placed such that the point of contact

between the specimen and the movable jaw of the clamp is the superior end plate of the vertebral body above the disc. Readings are collected over 2 minutes. The same process is repeated such that the scale readings are 20, 30 and 40 Kg. Finally, the screwing limb of the clamp is released to allow the scale reading to go back to 0 Kg. Pressure readings are collected while the intervertebral disc is regaining its neutral position.

- The specimen was allowed to remain in neutral position for 5-10 minutes prior to repeat the same experiment.

The above experiment is performed using six different specimens (all of sheep L5/6 spinal motion segment). By conducting those experiments, it is observed that results tend to vary, even when the same experiment is repeated using the same specimen. Therefore, for each specimen, the average was taken over multiple experiments. This was repeated until the 90% confidence intervals were satisfactory i.e., they did not vary significantly from the reported mean. In practice, this required repeating the same experiment between 5 to 10 times for each specimen. Next it is explained how the mean and confidence intervals are computed.

For any given specimen and each experiment, the results generated by the software record the changes in the pressure reading over time. Plotting these results generates a graph as is seen in Figure 4.20 (A) where the x-axis represents time and the y- axis represents the pressure sensor readings. Every such plot is typically stair-shaped, where the different steps reflects the different levels of deformation applied (see Figure 4.20 (B)). As can be observed, the pressure sensor readings fluctuate within each step. Therefore, the average reading for a given level is computed, as illustrated in Figure 4.20 (B). In so doing, the results can be simplified; the time factor can be excluded, leaving only the average pressure readings as a function of the level of deformation (see Figure 4.20 (C)). For the remainder of this section, the term “results” will be used to refer to the simplified results.

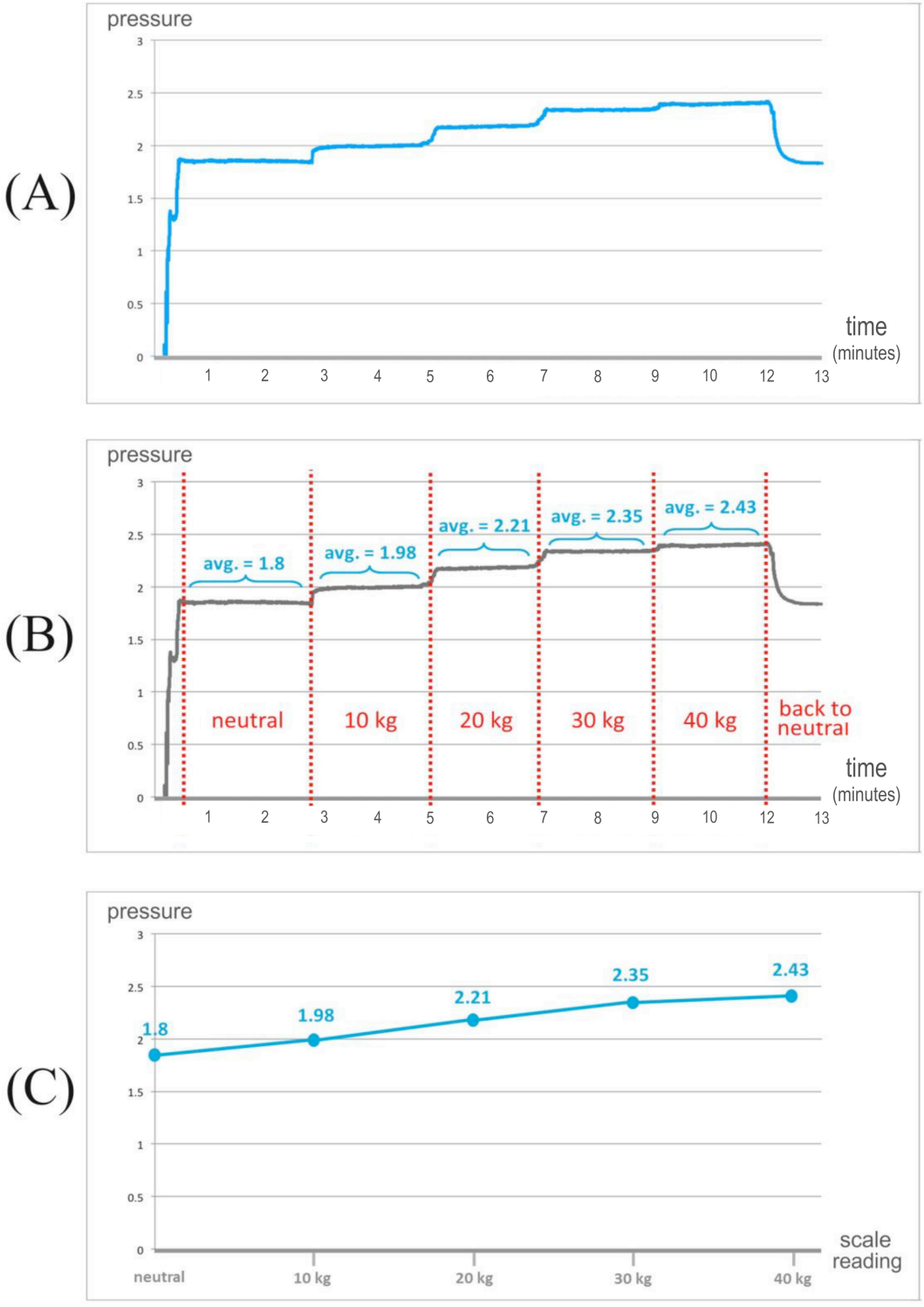

Figure 4.20 a typical result obtained from a single experiment on a single specimen. (A): pressure sensor reading over time. (B): the applied deformation and average pressure sensor reading in each step. (C): average pressure reading as a function of the level of deformation.

Figure 4.21 shows the average results obtained for the different specimens, where plot represents a single specimen. Here, the 90% confidence intervals are represented as error bars on the plots. Thus, showing the results in the form: $x \pm y$, means that the author is 90% confident that the true mean lies within the range of values: $x-y$ to $x+y$. For more details on how to calculate such confidence intervals, see [Altman et al., 2000].

As expected, there are differences in the results obtained for different specimens. This is due to the natural physical differences between the specimens. Nevertheless, it can be observed that the general broad trend remains similar for all specimens. In particular, the pressure sensor reading appears to grow linearly as with the quantity of the applied deformation. Moreover, the slop of the plot demonstrates the same broad trend, as shown in Figure 4.21.

With these experiments, the author demonstrated that:

1. Measuring the pressure with an intervertebral disc returns a positive reading.
2. The pressure within the nucleus pulposus increases when applying a deformation to the spinal motion segment.
3. Increasing the quantity of the deformation applied to the intervertebral disc results in a predictable alteration in its pressure.

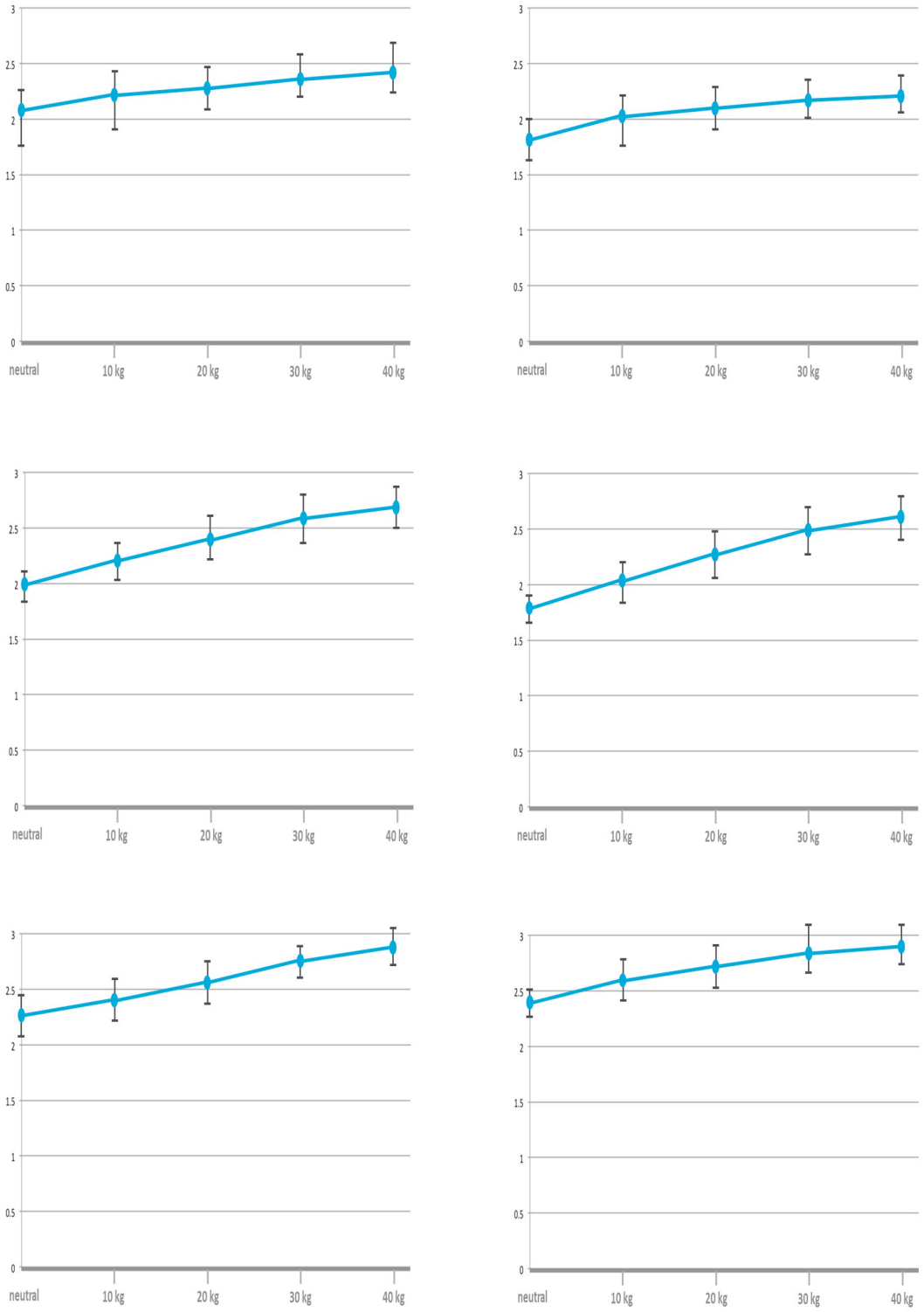

Figure 4.21 average results obtained from six different specimens (one plot per specimen). Error bars represents 90% confidence intervals.

Chapter 5
Conclusions and Future Work

Spinal musculoskeletal conditions are a social and financial burden for both the individuals as well as the society. Although these conditions are generally not fatal, they are often chronic. Axial spine pain—whether cervical, thoracic, or lumbar—is often attributed to disc degeneration. Furthermore, it has been shown that such degeneration is strongly linked to the changes in the intervertebral disc pressure. However, to date, the standard method for estimating this pressure suffer from being inaccurate and, more importantly, invasive. To address this issue, this dissertation took the first step towards providing a non-invasive alternative, which may use MRI scanners. In particular, to validate the applicability of these scanners as a tool for measuring intervertebral disc pressure, the following steps need to be taken: (1) modelling of the pressure measurement within the intervertebral disc, (2) obtaining an MR image for the same disc, and (3) comparing the two and finding whether a link exists between them. In this dissertation, the author developed, and validated, a layout suitable for in-vitro application to spinal motion segments.

Future work will focus on steps 2 and 3 of the proposed approach to validate the ability to use MRI scanners as a tool to measure the pressure within the intervertebral disc.

Appendix A: Risk Assessment Form

As mentioned earlier in Chapter 4, the experiments reported in this dissertation took place in a tissue lab, use of which requires a *risk-assessment form* to be completed, indicating any potential harm associated with each experiment, and to indicate the necessary precautions that are needed to minimize such risks. In particular, the following information needed to be specified in the form:

- **Activity** (any given task that may be associated with risk).
- **Event leading to potential harm**.
- **Harm** (that may be caused by the event).
- **Probability** (indicating how probable the harm is).
- **Severity** (indicating how severe the effect of the harm could be).
- **Control Measures** (the actions that could be taken to prevent potential harms).
- **Risk Acceptable (Yes/No)**: indicating whether potential risks are acceptable or whether this particular task should be avoided all together to avoid unacceptable risks.

The filled form, with all the potential harms, can be seen in Table 4.1.

Activity	**Event leading to potential harm**	**Harm**	**Probability**	**Severity**	**Control Measures**	**Risk Acceptable**	
						Yes	**No**
Obtaining animal specimens.	Contaminated material	Infection	Low	Potentially sever	Choose only fresh samples	Yes	
	Odor	Nausea, sickness and vomiting	Medium	Low	Keep well wrapped and covered	Yes	

	Handling the specimen	Infection	Low	Low	Use personal protective equipment (PPE)	Yes	
	Contamination of hands, clothing and surfaces	Infection	Low	Low	Use personal protective equipment (PPE)	Yes	
	Cutting and sectioning the specimens.	Sharps injury	Medium	Potentially sever	Suitable protectors i.e., gloves and eye protectors	Yes	
Preparation of the specimens	Cutting and sectioning the specimens.	Sharps injury	Medium	Potentially sever	**1.** Use of large trays regularly cleaned and decontaminated. **2.** Proper isolation of the specimens	Yes	
	Contamination to/from the surroundings including work bench, cloth or other specimens	Cross contamination leading to infection	Medium	Potentially sever	**1.** Use of large trays regularly cleaned and decontaminated. **2.** Proper isolation of the specimens	Yes	
	Inserting the needle in the specimen.	Sharps injury	High	Sever	Proper handling and disposing of sharps	Yes	
	Spillage of fluids on the floor, surfaces and near electrical circuits	Electric shock	High	Sever	**1.** Keep fluids in surroundings to a minimum. **2.** Regular drying of the surfaces and floors	Yes	

		Damage to instruments	High	Sever	**1.** Keep fluids in surroundings to a minimum. **2.** Regular drying of the surfaces and floors	Yes	
Freezing and storage of the specimens	Storage of the specimens at the lab freezers	Mixing with other samples	Low	Low	Storage in well labeled boxes suitable for freezer	Yes	
		Heavy weight samples after freezing	Low	Medium	Storage in well labeled boxes suitable for freezer	Yes	
		Compromise the results of other lab users	Low	Medium	Storage in well labeled boxes suitable for freezer	Yes	
		Samples deformed and axially loaded/ compressed in freezer	Low	Medium	Using the minimum number of samples required.	Yes	
	Defrosting samples	Liquid spillage	Low	Low	**1.** Proper sealing of the specimens. **2.** Using specially prepared trays for defrosting.	Yes	

Table 1: Risk-assessment form

Appendix B: Permission to Publish

Where applicable, the author sought a formal permission from the publisher, prior to the reproduction of any material used in the dissertation.

A copy of the permission letter can be seen in page 86.

ELSEVIER

Dear Amr Fahmy

We hereby grant you permission to reproduce the material detailed below at no charge **in your thesis, in print and on the University of** Southampton **web site** subject to the following conditions:

1. If any part of the material to be used (for example, figures) has appeared in our publication with credit or acknowledgement to another source, permission must also be sought from that source. If such permission is not obtained then that material may not be included in your publication/copies.

2. Suitable acknowledgment to the source must be made, either as a footnote or in a reference list at the end of your publication, as follows:

"This article was published in Publication title, Vol number, Author(s), Title of article, Page Nos, Copyright Elsevier (or appropriate Society name) (Year)."

3. Your thesis may be submitted to your institution in either print or electronic form.

4. Reproduction of this material is confined to the purpose for which permission is hereby given.

5. This permission is granted for non-exclusive world **English** rights only. For other languages please reapply separately for each one required. Permission excludes use in an electronic form other than as specified above. Should you have a specific electronic project in mind please reapply for permission.

6. Should your thesis be published commercially, please reapply for permission.

Yours sincerely

Jennifer Jones
Rights Associate

Bibliography

1. Adams M A and Hutton W C. The Effect Of Posture on the Fluid Content of Lumbar Intervertebral Discs. Spine (1983); 6:665-671.

2. Alini M, Eisenstein S M, Ito K, Little C A. Kettler A. Masuda K. Melrose J. Ralphs J. Stokes I and Wilke H J. Are Animal Models Useful for Studying Human Disc Disorders Degeneration? Eur Spine J. (2008); 17:2–19.

3. Altman, D. G., Machin, D., Bryant, T. N., and Gardner, M. J. (2000). Statistics with Confidence: Confidence Intervals and Statistical Guidelines. BMJ publishing group, London, UK.

4. ASTM (American Society for Testing and Materials) F 1469. Standard guide for conducting a repeatability and reproducibility study on test equipment for nondestructive testing (2004).

5. Bass E C, Duncan N A, Hariharan J S, Dusick J, Bueff H U and Lotz J C. Frozen Storage Affects the Compressive Creep Behavior of the Porcine Intervertebral Disc. Spine. (1997); 22:2867-2876.

6. Bogduk N, Tynan W, and Wilson A S. The Nerve Supply to the Human Lumbar IVD. J. Anat., (1981); 132:39-56.

7. Boszczyk B M, Boszczyk A A and Putz R. Comparative and Functional Anatomy of the Mammalian Lumbar Spine. The Anatomical Record J., (2001); 264:157–168.

8. Boutin P and Hogshead H. Surgical Pathology of the Intervertebral Disc. Is Routine Examination Necessary?. Spine, (1992); 17(10):1236- 1238.

9. Compere E L. Origin, Anatomy, Physiology and Pathology of the Intervertebral Disc. Instructional course lectures, (1961); 18:15-20.

10. Crock H V and Goldwasser M. Anatomic Studies of the Circulation in the Region of the Vertebral End-Plate in Adult Greyhound Dogs. Spine, (1984); 9:702-706.

11. Drake R L, Vogl W, and Mitchell W M, Gray's anatomy for students, (2010).

12. Elliott D M, Sarver J J. Young Investigator Award Winner: Validation of the Mouse and Rat Disc as Mechanical Models of the Human Lumbar Disc. Spine, (2004); 29:713–722.

13. Flynn J, Rudert M J. The Effects of Freezing and Freeze-Drying on the Biomechanical Properties of the Canine Interverteral Discs. Spine, (1990); 15:567-569.

14. Galante J. Tensile Properties of the Human Lumbar Annulus Fibrosus. Acta Orthop Scand, (1967); 100:91.

15. Giancoli D C. Physics: Principles with Applications, (2004);

16. Gleizes V, Viguier E, Féron1 J M, Canivet S. and Lavaste F. Effects of Freezing on the Biomechanics of the Intervertebral Disc. Surg Radiol Anat., (1998); 20:403-407.

17. Hendry N G C. The Hydration of the Nucleus Pulposus and Its Relation to Intervertebral Disc Derangement. JBJS, (1958);,40(B):132-144.

18. Humzah M D and Soames R W. The Human Intervertebral Disc: Structure and Function. The Anatomical Records, (1988); 220:337-356.

19. Hunter C J, Matyas J R, Duncan N A. The Notochordal Cell in the Nucleus Pulopsus: a Review in the Context of Tissue Engineering. Tissue Eng., (2003); 9:667–677.

20. Hutton W C. The Effect Of Hydrostatic Pressure on Intervertebral Disc Metabolism. Spine, (1999); 1507-1513

21. Jeffcoate I. Inside the Nucleus Pulposus. BMJ, (1977); 67-68.

22. Kettler A. L. Liakos B. Haegele H. and Wilke J. Are the Spines of Calf, Pig and Sheep Suitable Models for Preclinical Implant Tests?. Spine (2007); 16:2186–2192.

23. Kim H G, Shin D A, Kim H I, Yoo E A, Shin D G and Lee J O. Clinical and Radiological Findings of Discogenic Low Back Pain Confirmed by Automated Pressure-Controlled Discography. J Korean Neurosurg Soc., (2009); 46:333-339.

24. Malinsky J, The Ontogenetic Development of Nerve Terminals in the IVD of Man. Acta Anat., (1959); 38:96-113.

25. Matthews L S, Ellis D. Viscoelastic Properties of Cat Tendon: Effects of Time after Death and Preservation by Freezing. J. Biomech, (1968); 1:65-71.

26. Mc Nally D S and Adams M A. Internal Intervertebral Disc Mechanics as Revealed by Stress Profilmetry. Spine, (1992); 1:66-73.

27. Meryman T M. General principles of freezing and freezing injury in cellular materials. Annals of the New York Academy of Sciences, (1960); 85:503.

28. Mirza S K and White A A. Anatomy of Interveretebral Disc and Pathophysiology of Herniated Disc Disease, J Clin Laser Med Sur., (1995); 13(3):131-142.

29. Moore K L, Persaud TVN, and Torchia M G, The Developing Human Clinically oriented embryology, (2008); 338-339.

30. Nachemson A and Morris C J M. In Vivo Measurements of Intradiscal Pressure Discometry: a Method for the Determination of Pressure in the Lower Lumbar Discs. JBJS, (1964); 46:1077–1092.

31. Nachemson A L, The Load on Lumbar Disks in Different Positions of the Body. Clin Orthop Relat Res., (1966); 45:107-122.

32. Nachemson A L. Disc Pressure Measurements. Spine, (1981); 6(1):93-97.

33. Nachemson A. Measurement of Intradiscal Pressure. Acta Orthop Scand., (1959); 28:269–89.

34. Olmarker K. Animal Ethics in Basic Scientific Research.Eur Spine J., (1999); 8:85.

35. Panjabi M, Brown M, Lindahl S, Irstam L and Hermens M. Intrinsic Disc Pressure as a Measure of Integrity of the Lumbar Spine. Spine, (1988); 13:913-918.

36. Parke W W and Schiff D. The Applied Anatomy of the Intervertebral Disc. Orthop Clin North Am., (1971); 2:309-324.

37. Pederson H E, Blunck C F and Gardner F. The Anatomy of Lumbosacral Posterior Rami and Meningeal Branches of Spinal Nerves with an Experimental Study of Their Function. JBJS, (1956); 38:377-381.

38. Petter, C K. Methods of measuring the pressure of the intervertebral disc. J. Bone Joint Surg., (1933); 15:365.

39. Prithvi-Raj P. Intervertebral Disc: Anatomy-Physiology- Pathophysiology-Treatment. Pain Practice, (2008); 8(1):18-44.

40. Roofe P G. Innervation of Annulus Fibrosus and Posterior Longitudinal Ligament. Arch. Neurol. Psychiatry, (1940); 44:l00.

41. Sato K, Kikuchi S, Yonezawa T Y. In Vivo Intradiscal Pressure Measurement in Healthy Individuals and Patients with Ongoing Back Problems. Spine, (1999); 24:2468-2474.

42. Serrano Vela, R. La discographie. Confrontations Anatomo-Radio-Logiques et Cliniques dans 1'Etude du Desque Intervertebral Lorbaire. Thesis, Marseille, (1973).

43. Skaggs D L, Weidenbaum M, Iatridis J C, Ratcliffe A and Mow V C. Regional Variation in Tensile Properties and Biochemical Composition of the Human Lumbar Anulus Fibrosus. Spine. 1994;19:1310-1319.

44. Smith J W and Walmsley R. Experimental incision of the intervertebral disc. JBJS, (1951); 33(B):612-625.

45. Standring S, Ellis H, Healy J C, Johnson D, and Williams A, Gray's anatomy the anatomical basis of clinical practice, (2005); 736-798.

46. Stilwell D L. The Nerve Supply of the Vertebral Column and its Associated Structures in the Monkey. Anat. Rec., (1956); 125:139.

47. Taylor T K, Melrose J, Burkhardt D, Ghosh P, Claes L E, Kettler A and Wilke H J. Spinal Biomechanics and Aging are Major Determinants of the Proteoglycan Metabolism of Intervertebral Disc Cells. Spine, (2000); 25:3014–3020.

48. Terry Canale S. and Beaty J H. Disc and Spine Anatomy. In: Campbell's Operative Orthopaedics. New York: Mosby, (2007); 1350-1393.

49. Tichy J, Erhart J, Kittinger E and Privratska. Fundamentals of Piezoelectrical Sensorics: Mechanical, Dielecrtic, and Thermodynamical Properties of Piezoelecrtic Materials. Springer, (2010); 69-101.

50. Turner A. S. Spine Surgery in a Large Animal Model: Experiences and Limitations. European Cells and Materials, (2005); 10(3):34.

51. Wilke H J, Kettler A, Claes L E. Are Sheep Spines a Valid Biomechanical Model for Human Spines?. Spine. 1997(A); 22:2365–2374.

52. Wilke H J, Kettler A, Wenger K H and Claes LE. Anatomy of the Sheep Spine and its Comparison to the Human Spine. The Anatomical Record J. 1997(B); 247:542–555.

53. Wilke H J, Neef P, Caimi M, Hogland T and Claes L E. New In Vivo Measurements of Pressures in the Intervertebral Disc in Daily Life. Spine, (1999); 24(8):755-762.

54. Wilson J. Fundamentals of Pressure Sensing: Brush up on the Physics of Pressure and the Operating Principles of Pressure Senors. Sensors Journal [serial on the Internet], (2002) [cited 2002 July 1]; available from: http://www.sensorsmag.com/sensors/pressure/fundamentals-pressure-sensing-947

55. Wilson J. Pressure Measurment: Principles and Practice. Sensors Journal [serial on the Internet], (2003) [cited 2003 January 1]; available from: http://www.sensorsmag.com/sensors/pressure/pressure-measurement-principles-and-practice-969